Sun-induced Chlorophyll fluorescence and PRI improve remote sensing GPP estimates under varying nutrient availability in a typical Mediterranean savanna ecosystem

Oscar Perez-Priego[1]*, Jinhong Guan[1,2], Micol Rossini[3], Francesco Fava[3], Thomas Wutzler[1], Gerardo Moreno[4], Nuno Carvalhais[1,5], Arnaud Carrara[6], Olaf Kolle[1], Tommaso Julitta[3], Marion Schrumpf[1], Markus Reichstein[1] and Mirco Migliavacca[1]*

[1] Max Planck Institute for Biogeochemistry, Jena, Germany
[2] Chinese Academy of Sciences and Ministry of Water Resources, State Key Laboratory of Soil Erosion and Dryland Farming on Loess Plateau, Institute of Soil and Water Conservation, Yangling, Shaanxi, China
[3] Università degli Studi Milano-Bicocca, Remote Sensing of Environmental Dynamics Laboratory, DISAT, Milan, Italy
[4] Universidad de Extremadura, Forest Research Group, Plasencia, 10600, Spain
[5]Departamento de Ciencias e Engenharia do Ambiente, DCEA, Faculdade de Ciencias e Tecnologia, FCT, Universidade Nova de Lisboa, 2829-516 Caparica, Portugal
[6] Fundación Centro de Estudios Ambientales del Mediterráneo (CEAM), Valencia, Spain

Oscar Perez-Priego[1]**, email: opriego@bgc-jena.mpg.de

Jinhong Guan[1,2], email: *jguan@bgc-jena.mpg.de*

Francesco Fava[3], email: *francesco.fava@unimib.it*

Micol Rossini[3], email: micol.rossini@unimib.it

Thomas Wutzler[1], email: thomas.wutzler@bgc-jena.mpg.de

Gerardo Moreno[4], email: gmoreno@unex.es

Tommaso Julitta[3], email: tommaso.julitta@gmail.com

Nuno Carvalhais[1,5], email: ncarval@bgc-jena.mpg.de

Arnaud Carrara[6], email: arnaud@ceam.es

Olaf Kolle[1], email: olaf.kolle@bgc-jena.mpg.de

Marion Schrumpf[1], email: mschrumpf@bgc-jena.mpg.de

Markus Reichstein[1], *email: mreichstein@bgc-jena.mpg.de*

Mirco Migliavacca[1], *email: mmiglia@bgc-jena.mpg.de*

Running title: Remote sensing-based model of photosynthesis

Received: May 2015

Keywords: Photochemical reflectance index, sun-induced fluorescence, nutrient availability, photosynthesis, LUE model, dehesa.

*Corresponding Author
Biosphere-Atmosphere Interactions and Experimentation group
Biogeochemical Integration Department
Max Planck Institute for Biogeochemistry,
Jena
Germany
e-mail: opriego@bgc-jena.mpg.de

Abstract

This study investigates the performances of different optical indices to estimate gross primary production (GPP) of herbaceous stratum in a Mediterranean savanna with different Nitrogen (N) and Phosphorous (P) availability. Sun-induced chlorophyll Fluorescence yield computed at 760 nm (Fy760), scaled-photochemical reflectance index (sPRI), MERIS terrestrial-chlorophyll index (MTCI) and Normalized difference vegetation index (NDVI) were computed from near-surface field spectroscopy measurements collected using high spectral resolution spectrometers covering the visible near-infrared regions. GPP was measured using canopy-chambers on the same locations sampled by the spectrometers. We tested whether light-use efficiency (LUE) models driven by remote sensing quantities (RSM) can better track changes in GPP caused by nutrient supplies compared to those driven exclusively by meteorological data (MM). Particularly, we compared the performances of different RSM formulations -relying on the use of Fy760 or sPRI as proxy for LUE and NDVI or MTCI as fraction of absorbed photosynthetically active radiation (*f*APAR) - with those of classical MM.

Results showed higher GPP in the N fertilized experimental plots during the growing period. These differences in GPP disappeared in the drying period when senescence effects masked out potential differences due to plant N content. Consequently, although MTCI was tightly related to the mean of plant N content across treatment (r^2=0.86, *p<0.01*), it was poorly related to GPP (r^2=0.45, *p*<0.05). On the contrary sPRI and Fy760 correlated well with GPP during the whole measurement period. Results revealed that the relationship between GPP and Fy760 is not unique across treatments but it is affected by N availability. Results from a cross-validation analysis showed that MM (AIC_{cv}=127, ME_{cv}= 0.879) outperformed RSM (AIC_{cv}=140, ME_{cv}= 0.8737) when soil moisture was used to constrain the seasonal dynamic of LUE. However, residual analyses demonstrated that GPP predictions with MM are

inaccurate whenever no climatic variable explicitly reveals nutrient-related changes in the LUE parameter. These results put forward that RSM is a valuable means to diagnose nutrient-induced effects on the photosynthetic activity.

Abbreviations:
a, $\mathbf{a_0}$, and $\mathbf{a_1}$ are model parameters; $\mathbf{b_0}$, $\mathbf{b_1}$, $\mathbf{b_2}$, and $\mathbf{b_3}$ are fitting parameters of RSM; **EFPs**, ecosystem functional properties; ***f*(meteo),** limiting functions relying on meteorologically-driven data; ***f*APAR**, fraction of absorbed photosynthetically active radiation; ***f*PAIg**, fraction of *PAIg* in different plant forms; **Fy760**, sun-induced chlorophyll Fluorescence yield at 760 nm; **GPP**, gross primary productivity; $\mathbf{GPP_{noon}}$: instantaneous gross photosynthetic rate taken at solar noon (between 11:00 and 15:00 pm solar time); GPP_{daily}: mean value of the diurnal time course of gross photosynthetic rate; $\mathbf{GPP_{2000}}$, gross primary productivity estimated at 2000 of PAR; **LUE,** light use-efficiency; $\mathbf{LUE_m}$ potential or maximum LUE; **MM**, meteorologically driven model; **MM-VPD,** simplifier model of the original MOD17 that account for VPD in *f*(meteo); **MM(SWC-VPD)** meteorologically-driven model that account for VPD and soil moisture in *f*(meteo); **MTCI**, MERIS terrestrial-chlorophyll index; **NDVI**, Normalized difference vegetation index; **NEE**, net ecosystem CO_2 exchange; **PAIg**, Green Plant Area Index; **PAR**, Photosynthetically active radiation; ***ph***, physiologically-related parameter of RSM referring to either sPRI or Fy760 as a proxy for LUE; **PLRC**, photosynthetic light response curve; **PRI**, photochemical reflectance index; $\mathbf{R_{eco}}$, daytime ecosystem respiration; **RSM**, remote sensing based models; **SIF**, sun-induced chlorophyll fluorescence; **sPRI**, scaled-photochemical reflectance index; ***st***, structurally-related parameter of RSM referring to either NDVI or MTCI as a proxy for *f*APAR; **SWC**, soil water content; $\mathbf{SWC_{max}}$ parameter of the *f(meteo)* term; AL**VPD**, air-to-leaf vapor pressure deficit; **VPD**, vapor pressure deficit; $\mathbf{VPD_{max}}$ and $\mathbf{VPD_{min}}$ are fitting parameters of the *f(meteo)* term; $\boldsymbol{\alpha}$ is a parameter describing the photosynthetic quantum yield; $\boldsymbol{\beta}$ is the parameter that extrapolates to GPP at saturating light condition.

1. Introduction

Human-induced nutrient imbalances are affecting essential processes that lead to important changes in ecosystem structure and functioning (Peñuelas et al., 2013). In spite of the crucial role of nutrients in regulating plant processes, efforts to describe and predict the response of photosynthesis to such changes with remote sensing information have been limited. In the framework of the classical Monteith Light Use Efficiency (LUE) model (Monteith, 1972), estimates of photosynthesis (hereafter gross primary productivity, GPP) are based on three key quantities: i) the fraction of photosynthetically active radiation (*f*APAR) absorbed by the vegetation, ii) potential LUE (or maximum, LUE_m), normally taken from

look-up tables and associated with plant functional types (Heinsch et al., 2006) and iii) correction factors related to meteorological conditions that limit LUE_m. Although Nitrogen (N) deficiencies have been recognized one of the main correction factors of LUE_m (Madani et al., 2014), the predictive capability of LUE models is usually circumspect as they operate based on the general assumption that plants are under non-limiting nutrient conditions.

Very little attention has been given to nutrient-induced effects on *f*APAR and LUE in common formulations of LUE models. Light absorption by plant is given by chlorophyll pigments that enable photosynthetic processes. Assuming a correlation between leaf chlorophyll pigments and leaf N content, note that N atoms are basic components of the chlorophylls molecular structure, several studies have demonstrated that leaf N content can be estimated through chlorophyll-related hyperspectral vegetation indices (Baret et al., 2007; Schlemmer et al., 2013). Among these indices, the MERIS Terrestrial Chlorophyll Index (MTCI, Dash and Curran, 2004) has been used as a proxy for *f*APAR (Rossini et al., 2010; Wang et al., 2012). However, leaf N content is functional trait that controls GPP not only because it scales with chlorophylls but also regulates enzyme kinetic processes driving photosynthesis and hence the physiological status of the plant (Huang et al., 2004; Walker et al., 2014). Then, prescribing biome-specific LUE parameters and correcting LUE_m only for climatic and environmental conditions may hamper the accurate prediction of GPP (Yuan et al., 2014). For these reasons, recent literature has called for better physiological descriptors of the dynamic behavior of LUE (Guanter et al., 2014).

The sun-induced chlorophyll fluorescence (SIF) or physiological-related reflectance indices such as the photochemical reflectance index (PRI) provide a new optical means to spatially infer LUE (Damm et al., 2010; Guanter et al., 2014; Rossini et al., 2015) and can provide diagnostic information regarding plant nutrient and water status (Lee et al., 2013; Pérez-Priego et al., 2005; Suárez et al., 2008; Tremblay et al., 2012). From a physiological

perspective, the efficiency of green plants to transform absorbed light into chemical energy during photosynthesis can be characterized by two main photo-protective mechanisms: i) non-photochemical quenching that can be detected using the Photochemical Reflectance Index (PRI), originally proposed by (Gamon et al., 1992) to track changes in the de-epoxidation state of the xanthophyll cycle pigments, and ii) Chlorophyll fluorescence, the dissipation of energy that exceeds photosynthetic demand (Krause and Weis, 1984). The PRI has been directly correlated with LUE (Drolet et al., 2008; Gamon et al., 1997; Nichol et al., 2000; Peñuelas et al., 2011; Rahman et al., 2004). However, such relation may vary because of the sensitivity of the PRI to confounding factors like those associated with temporal changes in the relative fraction of chlorophyll:carotenoids pigment composition (Filella et al., 2009; Porcar-Castell et al., 2012), viewing angles and vegetation structure (Garbulsky et al., 2011; Grace et al., 2007; Hall et al., 2008; Hilker et al., 2008).

Alternatively, the estimation of SIF by passive remote sensing systems has been proven feasible in recent years from satellite (Frankenberg et al., 2014; Lee et al., 2013; Parazoo et al., 2014) to the field (Damm et al., 2010; Guanter et al., 2013; Meroni et al., 2011), and opens further possibilities to directly track the dynamics of LUE (Damm et al., 2010; Guanter et al., 2014). Although SIF correlates with LUE, such relations might not be conservative since chlorophyll fluorescence emission varies among species types (Campbell et al., 2008) or with stress conditions such as nutrient deficiencies (Huang et al., 2004; McMurtrey et al., 2003) or drought (Flexas et al., 2002; Pérez-Priego et al., 2005). Likewise with the PRI, the retrieval of SIF from the apparent reflectance signal is not trivial as long as it is affected by the vegetation structure or canopy background components (Zarco-Tejada et al., 2013).

Comparable spatial and temporal resolutions of radiometric and ground-based GPP measurements are essential to accurately optimize LUE model parameters, particularly in

heterogeneous ecosystems. Previous studies have related ecosystem-scale eddy covariance fluxes to radiometric measurements taken in single points to constraint LUE models. However, the explanatory power of LUE models might be greatly reduced by the spatial mismatch between radiometric and eddy covariance flux footprints (Gelybó et al., 2013; Porcar-Castell et al., 2015). Similar issues occur in small-scale factorial experiments where comparable measurements on an intermediate scale between leaf-scale cuvette measurements and ecosystem-scale eddy covariance measurements are required. Here, we tried to overcome such limitations by combining ground-based radiometric and CO_2 fluxes measurements with similar extension of the measurement footprint using portable spectrometers and canopy chambers in a nutrient-manipulation experiment.

The main objective of this study was to evaluate whether traditional LUE models driven by meteorological and phenological data (MM) entail a limited assessment of the environmental controls on GPP. More particularly, we evaluated if the effects of varying nutrient availability on GPP estimates as tracked by chlorophyll fluorescence and PRI can be equally explained by meteorology-driven models. To address the main objective we:

a) assess the effect of different nutrient supplies on grassland photosynthesis and optical properties and their relationships during a phenological cycle, including both growing and drying periods,

b) evaluate the performance of different LUE modeling approaches with varying nutrient availability and environmental conditions.

2. Material and Methods

2.1. Site description and experimental design

179 A Small scale nutrient Manipulation Experiment (SMANIE) was set up in a
180 Mediterranean savannah in Spain (39°56'24.68"N, 5°45'50.27"W; Majadas de Tietar, Caceres,
181 Fig. 1). The site is characterized by a mean annual temperature of 16^{o}C, mean annual
182 precipitation of ca. 700 mm, falling mostly from November until May, and by a very dry
183 summer. Similar to most Mediterranean grasland, grazing (<0.7 cows ha^{-1}) is the main land
184 use in the site. The site is defined as a typical Mediterranean savanna ecosystem, low density
185 of oak trees (mostly *Quercus Ilex* (L.), ~20 trees ha^{-1}) dominated by a herbaceous stratum.
186 The experiment itself was restricted to an open grassland area which was not influenced by
187 tree canopy. The herbaceous stratum is dominated by species of the three main functional
188 plant forms (grasses, forbs and legumes). The fraction of the three plant forms varied
189 seasonally according to their phenological status (Table 1). Overall, leaf area measurements
190 of the herbaceous stratum characterized the growing season phenology as peaking early in
191 April and achieving senescence by the end of May (Table 1).

192 The experiment consisted of four randomized blocks of about 20 m x 20 m. Each block
193 was separated into four plots of 9 m x 9 m with a buffer of 2 m in between to avoid boundary
194 effects. In each block, four treatments were applied (see Fig. 1):

195 (a) control treatment (C) with no fertilization;
196 (b) Nitrogen addition treatment (+N) with an application of 100 kg N ha^{-1} as potassium
197 nitrate (KNO_3) and ammonium nitrate (NH_4NO_3);
198 (c) Phosphorous addition treatment (+P) with an application of 50 kg P ha^{-1} as
199 monopotassium phosphate (KH_2PO_4); and
200 (d) N and P addition treatment (+NP), juxtaposing treatments (b) and (c).

201 Each fertilizer was dissolved in water and sprayed on foliage early in the growing season
202 (March 21st, 2014). The same amount of water used in the fertilizer solutions (~ 2 L m^{-2}) was
203 sprayed on the C treatment to avoid water imbalances among treatments.

Within each plot, two permanent, non-disturbed parcels (32 in total, see black squares in Fig 1) were dedicated to monitor CO_2 fluxes (net ecosystem CO_2 exchange, NEE; and daytime ecosystem respiration, R_{eco}). While NEE measurements were performed over the course of the day (from early in the morning to late afternoon), spectral measurements were conducted simultaneously with flux measurements only around noon on half of the parcels (16 in total).

Flux and spectral measurements were carried out in four field campaigns:

- Campaign #1: before fertilization (March 20th, 2014),
- Campaign #2: three weeks after fertilization (April 15th, 2014) during the peak of the growing period,
- Campaigns #3 and #4: on May 7th and 27th, 2014, respectively, concurring with the drying period were performed to evaluate joint effects related to physiological senescence processes.

Ancillary measurements were taken in every field campaign as follows: green plant area index (PAI_g) and aboveground biomass were directly measured by harvest in four parcels (0.25m x 0.25m) within each plot in the area surrounding that where spectral and flux measurements were taken. All samples were refrigerated just after collection, and transported for laboratory analyses. Fresh samples were separated into functional groups, the sample was scanned and green plant area was measured using image analysis (WinRHIZO, Regent Instruments Inc., Canada). Afterwards, fresh samples were dried in an oven at 65 °C for 48 hours and weighed to determine dry biomass. To analyze the nutrient content in leaf mass, biomass subsamples were ground in a ball mill (RETSCH MM200, Retsch, Haan, Germany) and total C and N concentrations were determined with an elemental analyzer (Vario EL, Elementar, Hanau, Germany). P concentrations were also measured: 100-mg biomass subsamples were diluted in 3 ml of HNO_3 65%, (Merck, Darmstadt, Germany) and microwave digested at high pressure

229 (Multiwave, Anton Paar, Graz, Austria; Raessler et al. (2005). Afterwards, elemental analysis
230 was conducted using inductively coupled plasma - optical emission spectrometry (ICP-OES,
231 Optima 3300 DV, Perkin Elmer, Norwalk, USA).
232
233 **2.2 Flux measurements and Meteorological data**
234 Net CO_2 fluxes were measured with three transparent chambers of a closed dynamic system.
235 The chambers consisted of a cubic (0.6m x0.6m x0.6 m) transparent low-density polyethylene
236 structure connected to an infrared gas analyzer (IRGA LI-840, Lincoln, NE, USA), which
237 measures CO_2 and water vapor mole fractions (W) at 1 Hz. The chambers were equipped with
238 different sensors to acquire environmental and soil variables, all installed at the chamber
239 ceiling: Photosynthetically Active Radiation (*PAR)* was measured with a quantum sensor (Li-
240 190, Li-Cor, Lincoln, NE, USA) placed outside of the chamber to be handled and leveled; air
241 and vegetation temperatures were measured with a thermistor probe (T_a, type 107, Campbell
242 Scientific, Logan, Utah, USA) and an infrared thermometer (T_c, IRTS-P, Apogee, UT, USA);
243 atmospheric pressure (P) was measured inside the chamber using a barometric pressure sensor
244 (CS100, Campbell Scientific, Logan, Utah, USA). The chambers were also equipped with soil
245 temperature and humidity sensors; soil water content was determined with an impedance soil
246 moisture probe (Theta Probe ML2x, Delta-T Devices, Cambridge, UK) at 5 cm depth and soil
247 temperature (type 107, Campbell Scientific, Logan, Utah, USA) at 10 cm depth. Saturation
248 vapour at surface temperature (i.e. Air-to-leaf vapour pressure deficit, VPD) was computed
249 using T_c and relative humidity, which was derived from water vapor molar fraction measured
250 with the IRGA (Perez-Priego et al., 2015).
251 The chamber operated as a closed dynamic system. A small pump circulates an air flow of 1 L
252 min^{-1} through the sample circuit: air is drawn from inside the chamber - through three porous-
253 hanging tubes spatially distributed through the chamber headspace - to the infrared gas

analyzer; this air flow is then returned to the chamber. The hanging tubes allowed spatially distributed sampling, obviating the need to homogenize air during chamber deployment. Nevertheless, one small fan (12V, 0.14A) was fixed at 0.3 m on a floor corner of the chamber and angled 45º upward.

A 0.6x0.6m metal collar was installed in each permanent parcel of each plot. The collar provided a flat surface onto which the bottom of the chamber was placed. The chamber was open and ventilated during 1 min prior to measurement, so that initial air composition and temperature in the confined environment of the chamber represented natural atmospheric conditions (as much NEE as Reco). For the NEE measurement, the transparent chamber was placed on the collar (closed position, lasted 3 minutes as a general rule), and fluxes were calculated from the rate of change of the CO_2 molar fraction (referenced to dry air) within the chamber. Similar procedure was carried out for R_{eco} but using an opaque blanket that covered the entire chamber and kept it dark during the measurements (PAR values around 0). Fluxes were calculated according to Pérez-Priego et al. (2015).

Shortly, the flux calculation algorithm reduces flux uncertainties (i.e. NEE and R_{eco}) by including the change-point detection method to determine the stabilization time, which defines the initial slope of the regressions, and a bootstrap resampling-based method to improve confidence in regression parameters and to optimize the number of data points used for flux calculation. In addition, a statistical analysis of residuals was performed to automatically detect the best fit among alternative regressions (i.e. quadratic, hyperbolic tangent saturating function, exponential, linear). These analyses were implemented in a self-developed R Package (available upon authors request or at the following link http://r-forge.r-project.org/projects/respchamberproc/). NEE and R_{eco} measurements were taken over the course of the day (from sunrise to sunset) for each field campaign. Chamber disturbance effects and correction for systematic and random errors (i.e. leakage, water dilution and gas

density correction, and light attenuation by the chamber wall) were applied according to Perez-Priego et al., (2015).

2.3 Field spectral measurements

Midday spectral measurements at canopy level were carried out under clear sky conditions using two portable spectrometers (HR4000, OceanOptics, USA) characterized by different spectral resolutions. Spectrometer 1, characterized by a Full Width at Half Maximum (FWHM) of 0.1 nm and a 700-800 nm spectral range was specifically designed for the estimation of sun-induced chlorophyll fluorescence at the O_2-A band (760 nm). Spectrometer 2 (FWHM = 1 nm, 400 - 1000 nm spectral range) was used for the computation of reflectance and vegetation indices. Spectrometers were housed in a thermally regulated Peltier box, keeping the internal temperature at 25°C in order to reduce dark current drift. The spectrometers were spectrally calibrated with a source of known characteristics (CAL-2000 mercury argon lamp, OceanOptics, USA) while the radiometric calibration was inferred from cross-calibration measurements performed with a calibrated FieldSpec FR Pro spectrometer (ASD, USA). This spectrometer was calibrated by the manufacturer with yearly frequency.

Incident solar irradiance was measured by nadir observations of a leveled calibrated standard reflectance panel (Spectralon; LabSphere, USA). Measurements were acquired using bare fiber optics with an angular field of view of 25°. The average canopy plane was observed from nadir at a distance of 110 cm (43 cm diameter field of view) allowing for collecting measurements of 50% of the surface area covered by the chamber measurements. The manual rotation of a mast mounted horizontally on the tripod allowed sequential observation of the vegetated target and the white reference calibrated panel. More in detail, every acquisition session consisted in the consecutive collection of the following spectra: instrument dark

current, radiance of the white reference panel, canopy radiance and radiance of the white reference panel. The radiance of the reference panel at the time of the canopy measurement was then estimated by linear interpolation.

For every acquisition, 3 and 10 scans (for Spectrometers 1 and 2, respectively) were averaged and stored as a single file. Five measurements were collected for each plot. Spectral data were acquired with dedicated software (Meroni and Colombo, 2009) and processed with a specifically developed IDL (ITTVIS IDL 7.1.1) application. This application allowed the basic processing steps of raw data necessary for the computation of the hemispherical conical reflectance factor described by Meroni et al. (2011).

The following indices were selected as suitable to investigate long term nutrient-mediated effects on photosynthesis. The NDVI (Rouse et al., 1974) was selected because it correlates well with plant area and among traditional spectral vegetation indices is used worldwide by classical LUE models as a surrogate for *f*APAR (Di Bella et al., 2004). The MTCI (Dash and Curran, 2004) was selected because it was specifically designed for canopy chlorophyll content estimation, and recently used as proxy for *f*APAR as well as NDVI. In this study we used the PRI and SIF as surrogates for LUE. A scaled PRI (sPRI) calculated as (PRI+1)/2 was used. SIF was estimated by exploiting the spectral fitting method described in Meroni et al. (2010), assuming linear variation of the reflectance and fluorescence in the O_2-A absorption band region. The spectral interval used for SIF estimation was set to 759.00 - 767.76 nm for a total of 439 spectral channels used. For methodological distinction among existing approaches, hereafter SIF is referred to as F760. Because F760 is affected by PAR we use the apparent chlorophyll fluorescence yield (Fy760; Rossini et al., 2010) computed as the ratio between F760 and the incident radiance in a nearby spectral region. A summary of the

formulation to compute the vegetation indices and their corresponding target and proxy in the LUE model approach are presented in Table 2.

2.4 Relationship between GPP and remote sensing data

Ecosystem-level GPP was computed as the difference between NEE and daytime R_{eco} taken consecutively with the chambers. To assess how GPP is modulated by light among treatments and over the phenological cycle of the herbaceous stratum, we computed the parameters of photosynthetic light response curve (PLRC). Specifically, the Michaelis–Menten function was fitted to GPP and PAR data taken throughout the course of the day (from sunrise until sunset) for each field campaign and treatment as follows:

$$GPP_i = \frac{\alpha \times \beta \times PAR_i}{\beta + PAR_i \times \alpha}, \quad [1]$$

where α is a parameter describing the photosynthetic quantum yield (μmol CO_2 μmol photons^{-1}), and β is the parameter that extrapolates to GPP at saturating light condition (μmol CO_2 m^{-2} s^{-1}). According to Ruimy et al. (1994), we used the optimized parameters of the PLRC as defined in Eq. (1) to estimate the GPP at 2000 μmol quantum m^{-2} s^{-1} of PAR (hereafter referred to GPP_{2000}).

We evaluated direct relationships between those GPP measurements taken around noon (between 11:00 and 15:00 pm solar time) with the chamber (GPP_{noon}) and sequentially measurements of Fy760 and spectral indices (NDVI, sPRI, MTCI). In addition, to avoid confounding factors in the relationship between Fy760 and sPRI and photosynthesis, we also used GPP_{2000} as a maximum photosynthetic capacity descriptor.

2.5 Monteith's light-use efficiency modelling approaches

Following Monteith's LUE framework (Eq. 2) two alternative modeling approaches were used:

$$GPP = LUE \times fAPAR \times PAR, \quad [2]$$

i. ***Meteo-driven methods (MM);*** based on the MOD17 formulation, fAPAR is approached through the relationship with NDVI and includes limiting functions f(meteo), which are based on climatic driving parameters to limit maximum LUE (LUE_{max}). Alternatively, Eq. (2) was reformulated as follows:

$$GPP = LUE_{max} \times f(meteo) \times (a_0 \times NDVI + a_1) \times PAR, \quad [3]$$

where LUE_{max}, a_o, and a_1 are model parameters. Three different f(meteo) functions were tried;

a) **MM-VPD,** this method is a simplification of the original MOD17, in which *f*(meteo) includes two linear ramp functions of both maximum and minimum vapour pressure deficit (VPD) and minimum temperature (T). Please note that in this study, vapor pressure deficit of the ambient air used in MOD17 is replaced by leaf-to-air vapour pressure deficit, which is defined by plant temperature and used as a better descriptor of plant physiology. Since minimum temperature was not limiting at the site, we fixed the *f*(meteo) parameters as suggested by Heinsch et al. (2006) but constraining only a function based on VPD as follows:

$$f(meteo) = \left[1 - \left(\frac{VPD - VPD_{min}}{VPD_{max} - VPD_{min}}\right)\right], \quad [4]$$

then, VPD_{max} and VPD_{min} are defined as the three parameters of the *f(meteo)* term.

b) **MM-SWC**, where *f*(meteo) includes a soil water content (SWC) function (Migliavacca et al., 2011) as the limiting factor of LUE_{max}:

$$f(meteo) = \frac{1}{1 + exp^{(SWC_{max} - a \times SWC)}}, \quad [5]$$

here, SWC_{max} and *a* are defined as the parameters of the *f(meteo)* term.

c) **MM (SWC-VPD)**, where *f*(meteo) includes both soil water content and VPD functions as limiting factors:

$$f(meteo) = \left[1 - \left(\frac{VPD - VPD_{min}}{VPD_{max} - VPD_{min}}\right)\right] \times \left[\frac{1}{1 + exp^{(SWC_{max} - a \times SWC)}}\right], \quad [6]$$

here, VPD_{max}, VPD_{min}, SWC_{max} and *a* are defined as the parameters of the *f(meteo)* term.

ii. ***RS-based method (RSM)****;* based on a solution of Eq.(1) as follows:

$$GPP = LUE \times fPAR \times PAR = (a_0 \times Ph + a_1) \times (a_2 \times St + a_3) \times PAR$$

$$= (b_0 \times Ph + b_1 \times St + b_2 \times Ph \times St + b_3) \times PAR\ , \quad [7]$$

where four alternative model formulations were obtained from the combination of the sPRI or Fy760 as the physiological related proxy (*Ph*) for LUE, and NDVI or MTCI as structural-related (*St*) proxy for *f*APAR. In Eq. 7, b_0, b_1, b_2, and b_3 are fitting parameters (Rossini et al., 2010).

2.5 Statistical analysis and model performance

All model formulations were optimized using GPP_{noon} and spectral measurements taken at midday. Since the means of spectral measurements per treatment could have unequal variance, a Welch's t-test was performed to evaluate significant differences between the mean values of the different vegetation indices for each treatment and over the four field campaigns. In addition, an analysis of covariance (ANCOVA) was used to test whether or not there was a significant interaction by the treatment effect between GPP_{noon} and Fy760 and different spectral indices. Like vegetation indices, a t-test was performed to the daily average of GPP taken over the course of the day (GPP_{daily}).

2.5.1 Cross-validation analyses and model evaluation

Different model formulations were evaluated in leave-one-out (loo) cross-validation: from the whole dataset composed by *n* observations, one data point at a time was removed. The model was fitted against the $n-1$ remaining data points (training set) while the excluded data (validation set) were used for model evaluation. The cross-validation process was then repeated *n* times, with each of the *n* observations used exactly once as the validation set. For each validation set of the cross-validated model, statistics were calculated.

Model accuracy was evaluated by means of different statistics according to Janssen and Heuberger (1995): root mean square error (RMSE), relative root mean square error (rRMSE) determination coefficient (r^2) and model efficiency (ME). The model performances in loo cross-validation were also calculated and reported as $RMSE_{cv}$, $rRMSE_{cv}$, r^2cv and ME_{cv}.

The Akaike Information Criterion (AIC_{cv}) was used to evaluate the trade-off between model complexity (i.e. number of parameters) and explanatory power (i.e. goodness-of-fit) of the different model formulations proposed. The AIC_{cv} is a method based on information theory that is useful for statistical and empirical model selection purposes (Akaike, 1998). Following Anderson et al. (2000), in this analysis we used the following definition of AIC_{cv}:

$$AIC_{cv} = 2(\rho + 1) + n\left[ln\left(\frac{RSS_{cv}}{n}\right)\right] \quad [8]$$

where *n* is the number of samples (i.e. observations), *p* is the number of model parameters and RSS_{cv} is the residual sum of squares divided by n.

The LUE model formulations proposed in Section 2.4 can be ranked according to AIC_{cv}, where the model with lowest AIC_{cv} is considered the best among the different model formulations.

All model parameters (MM, and RSM) were estimated by using a Gauss-Newton nonlinear least square optimization method (Bates and Watts, 2008), and standard errors of parameters

were estimated by bootstrapping (number of sampling, n = 500; Efron and Tibshirani (1994)), both implemented in the R standard package (R version 3.0.2, R Development Core Team, 2011).

3. Results

3.1 Effects of fertilization on plant nutrient contents and GPP

Fertilization caused strong variations in leaf N and P content among treatments, plant forms and across field campaigns (Table 2); while total N content in plants ranged slightly between 13.8±1.2 and 15.4±1.7 mg g^{-1} for the C and +P treatments over the whole experiment, the largest increases in total N content were found in the peak of the growing season (#2, March 20th, 2014), when +NP and +N treatments reached values of up to 23.7±2.0 and 23.5±4.1 mg g^{-1}, respectively. Although slightly lower, the differences in total N content between C and +P, and +NP and +N remained high over the drying period. Total P content was higher in +NP and +P treatments after fertilization, as compared to +N and C treatments. Consequently, the N:P ratio at the first campaign after fertilization (#2) achieved values of up to 14.2, 6.6, 6, and 3.7, in +N, C, +NP, and +P treatments, respectively. Similar differences in N:P between treatments were also observed during the drying period (#3 and #4, Table 2). On the other hand, PAI_g ranged from 0.4 m^2 m^{-2} in campaign #4 to up to 2.5 m^2 m^{-2} in campaign #2. No differences were found in PAI_g among treatments since grazing apparently offset any potential difference in the green aboveground production. Regarding variations in the fraction of plant forms, no significant differences were found between treatments.

Fertilization caused significant differences in the GPP_{daily} ($p<0.05$) between N-addition treatments (mean values of 19.62±4.15 and 18.19±5.67 μmolCO_2 m^{-2} s^{-1} for +N and +NP, respectively) and C and +P treatments (14.31±5.39 and 14.40±4.09 μmolCO_2 m^{-2} s^{-1}, respectively) in the peak of the growing season (campaign #2); a relative difference of 37% in

442 GPP_{daily} values was found between +N and +NP and C treatments. During the drying period,
443 however, GPP was substantially down regulated (campaigns #3 and #4) and no significant
444 differences were found in GPP_{daily}, regardless of differences in plant N content observed
445 among treatments. The potential photosynthetic capacity GPP_{2000} (Fig 2) derived from PLRC
446 was similar in the four treatments in the pretreatment period (campaign #1, Fig 2a). GPP_{2000}
447 varied throughout the season and peaked in the campaign #2 (April 15th) in all treatments. At
448 this time PLRC of the +N and +NP treatments diverged clearly from no N addition treatments
449 (C and +P, Fig 2b). GPP_{2000} was higher in +N and +NP treatments (18.6 and 20.1μmol CO_2 m^{-2}
450 s^{-1}, respectively) compared to C and +P treatments (14.9 and 15.4 μmol CO_2 m^{-2} s^{-1},
451 respectively). After campaign #2, when the soil layer at 5 cm depth dried out appreciably
452 (volumetric water content achieved values of 3% vol., data not shown), vegetation
453 progressively senesced and GPP_{2000} in turn was down-regulated and converged to similar
454 values in all treatments, regardless the higher N content observed in +N and +NP treatments
455 as compared with C and +P treatments (Table 1). During the drying season, GPP_{2000} decreased
456 in all treatments ranging between 5.6 and 8 μmolCO_2 m^{-2} s^{-1} and no differences among
457 treatments was observed (Fig 2 c and d). These results indicate that the senescence of the
458 herbaceous stratum, which is regulated by water availability, strongly modulated the
459 photosynthetic capacity of the vegetation over the season.

460

461 **3.2 – Effects of fertilization on remote sensing data**

462 Optical properties of the analyzed plots were similar during campaign #1, before the
463 nutrient application. A pronounced seasonal time course was observed for both *Ph* (sPRI and
464 Fy760) and structural indices (*St*; NDVI and MTCI) with maximum values during the second
465 campaign. It is interesting to note that while for *St* indices the maximum values were reached
466 in +N plots, +NP plots showed maximum *Ph* values. Vegetation indices and Fy760 then

decreased in the drying period (Figure 3). As for GPP, differences between treatments were more evident during campaign #2 when C plots showed statistically lower values for all the indices considered, while only MTCI was able to detect significant differences between N fertilized plots (+N and +NP). Furthermore significant differences in Fy760 and MTCI between C and the other three treatments were found ($p<0.05$) in the drying period (campaign #4,). NDVI varied significantly with changes in PAI_g with values of 0.4 in the campaign #4 up to 0.8 in the campaign #2 ($p<0.001$, $r^2=0.79$).

3.3 Relationship between remote sensing data and GPP

While *Ph* indices (Fy760 and sPRI) varied linearly with GPP_{noon} in all treatments ($p<0.001$, $r^2=0.66$ for Fy760 and $p<0.001$, $r^2=0.79$ for sPRI, respectively, Fig 4 a and b,), different patterns were observed for *St*: NDVI and GPP were best fitted by an exponential regression ($p<0.001$, $r^2=0.77$ Fig 4 c), while a weak linear relationship between MTCI and GPP_{noon} ($p<0.05$, $r^2=0.45$, Fig 4 d) was found. Although a weak relation between MTCI and GPP_{noon} was found, MTCI was strongly correlated with plant N content ($y=14.17x-2.49$, $p<0.001$, $r^2=0.86$). Note that these results are computed excluding data taken in the pre-treatment campaign (#1) and differences in the relationship between remote sensing data and GPP_{noon} among treatments can be only attributed to nutrient-induced effects. The ANCOVA test did not show significant differences neither in slope nor intercept of the relationship between GPP_{noon} and sPRI, and NDVI across treatments. However, barely significant differences were found in the relationship between GPP_{noon} and Fy760 ($p<0.1$, Fig 4b) and significant between GPP_{noon} and MTCI ($p<0.01$, Fig 4d) between N addition treatments (+N and +NP) and C treatments (C and +P).

Similar to GPP_{noon}, GPP_{2000} was also significantly related to mean midday sPRI (r^2=0.76, p<0.001, Fig. 5a) and Fy760 (r^2=0.76, p<0.001, Fig. 5b). As expected, an exponential regression fitted best for NDVI, while a poor relationship with MTCI was found (data not shown).

3.4 Modeling GPP

Based on the AIC_{cv} criterion, MM (VPD- SWC) outperformed MM-VPD, MM-SWC and RSM models. Although MM (VPD-SWC) showed high accuracy in the predictions (ME_{cv}=0.879, r^2_{cv}=0.881), this model had a tendency to underestimate observation at high GPP_{noon} values (see comparison between model predictions and observations, Figures 6a-6c). Note that the highest biases in modeled GPP_{noon} values among MM models belong to +N and +NP treatments in field campaign #2. Since the four treatments experienced the same environmental conditions (i.e. comparable values of SWC, VPD, air temperature), this bias can be attributed to the higher N content (+N and +NP treatments) as compared to C and +P treatments. Remarkably, residuals of the MM (VPD-SWC) taken from periods with moist soil (SWC>15) were significantly correlated with sPRI and Fy760 (p<0.05, Fig. 7 a and b, respectively). However, no biases between residuals and predictions were observed in RSM over the span of values and treatments (Fig. 8). Results from the evaluation of model performance indicated that RSM performs best when NDVI rather than MTCI, is used as *St* in the Eq.7 and, hence, as a proxy for *f*APAR (Table 3). Our results indicated that RSM performs best when either *Ph* (sPRI or Fy760) is combined with NDVI as *St*.

4. Discussion

4.1 Effects of nutrients on GPP and remote sensing data and their relationships

514 Nutrient fertilization, particularly N inputs, induced physiological changes manifested as an
515 increase in photosynthetic capacity under high light conditions (Fig. 2; Hirose and Werger
516 (1994). As we expected, plant N content showed to be a trait of photosynthesis that influences
517 a variety of aspects of photosynthetic physiology (Ciompi et al., 1996; Sugiharto et al., 1990).
518 These physiological changes were reflected on the optical properties, particularly on
519 fluorescence and sPRI. The increase in fluorescence with N fertilization inputs was recently
520 explained as the combined effect that a higher N content has on 1) chlorophyll content, which
521 magnifies APAR and enhances fluorescence signal, and on 2) the increased photosynthetic
522 capacity that results in reduced NPQ activity and consequently increases the fluorescence
523 signal (Cendrero-Mateo et al., 2015).The relationships between GPP_{noon} and Fy760 is not
524 unique and may vary from optimal to non-optimal environmental conditions (i.e. nutrient
525 deficiencies, water stress), when other regulatory mechanisms might reduce the degree of
526 coupling between fluorescence and photosynthesis (Cendrero-Mateo et al., 2015; Porcar-
527 Castell et al., 2012). Although Fy760 was positively correlated with GPP_{noon}, barely
528 significant differences in the slope of this relationship were observed between treatments (Fig.
529 4 b). Further studies are needed to fully explore the relationship between Fy760 and GPP_{noon}
530 under different stress conditions and over different ecosystems. However, if confirmed, the
531 effect of nutrient availability on the relationship between Fy760 and GPP_{noon} could have
532 important implications in GPP modeling. This result suggests that the inclusion of a
533 correction factor related to leaves N:P stoichiometry should be considered when modeling
534 GPP assuming a linear relationship with fluorescence at plant functional type level (Guanter
535 et al., 2014; Joiner et al., 2013).

536 In this study we also explored the capability of remote sensing to describe ecosystem
537 functional properties defined as those quantities that summarize and integrate ecosystem
538 processes and responses to environmental conditions and can be retrieved from ecosystem

level fluxes (e.g. GPP_{2000}) and structural measurements (Reichstein et al., 2014). GPP at light saturation (i.e. GPP_{2000}) is one example of an ecosystem functional property, shown here to be quite correlated to sPRI and Fy760 (Fig. 5). This result suggests that sPRI and Fy760 open also new opportunities for remote sensing products to describe the spatiotemporal variability of essential descriptors of ecosystem functioning (Musavi et al., 2015). Inferring GPP_{2000} using remote-sensing has important implication both for monitoring global carbon cycle and for benchmarking terrestrial biosphere models.

MTCI was tightly related with N content (r^2=0.86, p<0.001), independent of other structural variables (i.e. PAI_g), and can be used as a good indicator of N availability. Although MTCI has been proven to be very sensitive to variations in chlorophyll contents (Dash and Curran, 2004) and hence linkable with light absorption processes, it was weakly correlated with GPP, particularly in plots added with N (+N and +NP; r^2=0.27, p<0.01, Fig 4 d). A quite wide range of GPP_{noon} values were found at high values of MTCI – high GPP_{noon} values corresponding to the growing season and low ones to the drying period – which can be explained by two simultaneous mechanisms.

First, despite the high plant N content, physiological mechanisms including stomatal control or reduced carboxylation efficiency down-regulate GPP (Huang et al., 2004) and ultimately might break the relationship between GPP_{noon} and MTCI. Second, MTCI tracks changes in N content regardless changes in canopy structure occuring during the dry season when grass achieved senescence (i.e. green to dry biomass ratio, PAI_g). More studies aimed at the separation of the combined effects of N and changes in green/dry biomass fractions on *f*APAR are essential. On the other hand, although NDVI followed the seasonal dynamic of PAIg, it saturated at high GPP_{noon} values indicating the low ability of this index to detect spatial variations induced by N fertilization.

563 Although optical measurements were taken at high spatial resolution (<0.36 m^2), the
564 separation of confounding factors affecting sPRI or Fy760 is essential to elucidate the
565 mechanistic association between sPRI or Fy760 and GPP. Like sPRI, the retrieval of Fy760
566 from the apparent reflectance signal can be also affected by vegetation structure or canopy
567 background components (Zarco-Tejada et al., 2013). After optimization and selection of the
568 best model parameters using NDVI and sPRI (or Fy760) as driver, we analyzed the response
569 of simulated GPP to variations in NDVI and sPRI (or Fy760, Fig 9). Results indicate that at
570 high GPP levels, Fy760 and sPRI but less NDVI shaped GPP. However, at low GPP levels,
571 either Fy760 or sPRI responded to GPP on a small scale (Fig 9b). Figure 9 suggests that the
572 relationship between NDVI and sPRI or Fy760 is not unique and NDVI may play an
573 important role in driving GPP in ecosystem characterized by marked seasonal variations. Our
574 results highlight the complementarity between NDVI and Fy760 or sPRI. Particularly, NDVI
575 assisted Fy760 or sPRI in predicting GPP under conditions with low biomass (i.e. low LAI),
576 when confounding factors may affect Fy760 or sPRI. In semi-arid ecosystems, the lack of
577 sensitivity of sPRI or Fy760 to changes in GPP during dry conditions have been explained by
578 the soil background effect on the reflectance signal (Barton and North, 2001; Mänd et al.,
579 2010; Zarco-Tejada et al., 2013). Accordingly, Rahman et al., (2004) pointed out that
580 conditions where sPRI performs best are in dense canopies with low portion of bare soil.

581

582 **4.2 Performances of different LUE modeling approaches.**

583 Here we aim at answering the question how can we better simulate GPP using LUE modeling
584 with varying nutrient availability and environmental conditions by drawing comparisons
585 between the two model philosophies; RSM against MM approaches. There are an increasing
586 number of studies focused on the development of LUE models driven by remotely sensed
587 information to better explain spatio-temporal variations of GPP (Gitelson et al., 2014; Rossini

et al., 2012; Rossini et al., 2014). However, nutrient availability (and in particular N) greatly influence the spatial variability of LUE even within the same plant-functional type (e.g. grasslands) and further studies are essential. The slightly better performance in cross validation of the MM (VPD-SWC) against all model configurations, including RSM, supports the importance of a joint use of SWC and VPD as key parameters to constraint LUE in arid and semi-arid ecosystems (Prince and Goward, 1995). However, residual analyses demonstrated that MM (VPD-SWC) was unable to track N-induced differences in GPP during the growing period, when both parameters are not limiting (Fig. 7). By contrast, accurate estimates of GPP were obtained with RSM both over the drying and the growing periods. These results also indicate the importance of physiological descriptors to constrain LUE, which prevails over structural factors controlling *f*APAR (i.e. green biomass) under given environmental conditions and encourage the use of hyperspectral remote sensing for diagnostic upscaling of GPP.

With sPRI or Fy760 as a proxy for LUE, RSM is presented as a valuable means to diagnose N-induced effects on physiology. Our results show the limits of MM in predicting the spatial and temporal variability of GPP when LUE is not controlled by meteorological drivers alone (VPD, temperature, soil moisture)**.** Accordingly, GPP is eventually biased whenever neither climatic nor structural state variables explicitly reveal spatial changes in the LUE parameter associated with plant nutrient availability; residuals showed a clear tendency to underestimate the highest modeled GPP values, significantly correlated to Fy760 and sPRI (Fig.7). From a practical point of view, the forcing variables of RSM approaches may show a better observational coverage. In effect, the satellite-based retrievals of RSM forcing variables could additionally overcome representativeness limitations and potential regional or seasonal biases in meteorological fields (Dee et al., 2011). The uncertainties in forcing variables of MM (i.e. temperature, VPD and soil moisture) could propagate and affects the GPP estimates.

5. Concluding remarks

1. Fy760 and sPRI correlated well with GPP: both increased with N content and decreased with senescence.
2. MTCI can be used as a good descriptor of N content in plants but the relationship with GPP breaks down under drought conditions.
3. Meteo-driven models were able to describe temporal variations in GPP, and soil moisture can be a key parameter to better track the seasonal dynamics of LUE in arid environments. However, meteo-driven models were unable to describe N-induced effects on GPP. Important implication can be derived from these results and uncertainties in the prediction of global GPP still remain when meteo-driven models do not account for plant nutrient availability.
4. sPRI or Fy760 provide valuable means to diagnose nutrient-induced effects on the photosynthetic activity and, therefore, should be included in diagnostic GPP models.

Author contribution

OPP, MM, and MRo conceived the analyses, wrote the introduction, results and discussion, and led the preparation and revision of the manuscript; FF, TJ made hyperspectral measurements, computed spectral indices and fluorescence, and wrote part of the methods section; JH, MS and OPP made chamber measurements, soil and vegetation lab analysis and wrote part of the methods section; JH organized the dataset; OK provided technical assistance in the design and construction of the chambers and data acquisition system and wrote part of the methods section; GM and AC designed the fertilization protocol, organized sampling, provided technical assistance for the managing of the experiment and contributed to data interpretation; TW and OPP developed the R package for flux calculations, computed GPP and flux uncertainties and contributed to statistical analyses and interpretation. NC and MRe contributed to analyses and interpretation and to draft the manuscript. All authors discussed the results and contributed to the manuscript.

Acknowledgements

The authors acknowledge the Alexander von Humboldt Foundation and the Max Planck Research Award that is funding the research activity. We acknowledge City council of Majadas de Tietar for its support. The authors acknowledge Andrea Perez-Bargueno, and Enrique Juarez-Alcalde from (University of Extreamdura), Ramon Lopez-Jimenez (CEAM), Kathrin Henkel, and Martin Hertel from (MPI-Jena) and Marco Celesti (UNIMIB) for the support in the field, lab analysis and the development of the transparent chambers; Javier Pacheco Labrador and Maria Pilar Isabel Martin (CSIC) for help calibrating the radiometric system. We thank Professor Andrew S. Kowalski (University of Granada, Spain) for his review of the manuscript and constructive comments.

Figure Captions

Fig 1. Overview of the experimental site (SMANIE): the experimental blocks are drawn on an image acquired with the hyperspectral AHS (Sensytech Inc., Beverly, MA, USA) sensor during April 2014.

Fig 2. Photosynthetic light response curves derived for each growing period: (a) pretreatment and (b) post-treatment and drying periods (c and d). Treatments are presented in different colors. Lines represent the Michaelis–Menten function fitting gross photosynthesis (GPP, $\mu molCO_2 m^{-2} s^{-1}$) and photosynthetic active radiation (PAR, $\mu mol m^{-2} s^{-1}$).

Fig 3. Seasonal time course of mean midday physiologically-driven vegetation indices; (a) scale photochemical reflectance index, sPRI (b) apparent fluorescence yield (Fy760), and structure-driven vegetation indices, (c) NDVI, and (d) MTCI among C, +N, +NP and +P treatments in a Mediterranean grassland in Spain. Bars indicate standard deviation, N = 4. Different letters denote significant difference between treatments (Weilch t test, $P < 0.05$).

Fig 4. Relationship between GPP_{noon} and remote sensing data: (a) scaled photochemical reflectance index (sPRI), (b) apparent fluorescence yield, (c) normalized difference vegetation index (NDVI), and (d) MTCI. Square symbols represent measurements taken in the pre-treatment (#1) and circles after fertilization (#2–#4). Data were obtained at midday and lines represent results from the regressions for each treatment excluding measurements in the pre-treatment.

Fig 5. Relationship between GPP2000 and average values of sPRI and (b) apparent fluorescence yield (Fy760). Lines represent results the best linear regressions fitting the data.

Fig 6. Comparison between measured GPP and GPP modeled with the best performing LUE model for each kind of formulation: MM (VPD, panel a), MM (SWC, panel b), MM (including VPD and SWC, panel c), RSM (sPRI-NDVI panel d), and RSM (Fy760-NDVI, panel e). Results from the cross-validation analysis are presented in Table 3.

Fig 7. Correlation between residuals of the MM (VPD-SWC) model and (a) scaled photochemical reflectance index (sPRI) and (b) chlorophyll fluorescence yield (Fy760) taken from periods with high soil water content (SWC>15%, red circles). No correlation was observed when SWC<15% ($p>0.5$, black circles).

Fig 8. Plot between residuals of both the Meteo-driven model (MM-VPD) and Remote Sensing-based method (RSM) and modeled GPP values. Both lines represent the local polynomial regression fitting of the residuals against predicted values.

Fig 9. Contour plot indicating how variation in photosynthesis (GPP, $\mu mol\ CO_2\ m^{-2}\ s^{-1}$) are explained by variations in the LUE and fPAR parameters of the RSM. While (a) sPRI and (b) Fy760 are indistinctly used as a proxy of LUE, the NDVI is taken as *f*PAR.

Table Captions

Table 1. Ancillary data resulting from the analysis. Green Plant Area Index (PAIg), fraction of PAI in different plant forms (fPAI), and C, N, and P plant content. The N:P ratio also is shown. Data correspond to the mean value and standard deviation (SD) of the subsamples taken in each plot and treatment.

Table 2. Spectral vegetation indices computed in this study. Vegetation indices are classified into two major classes based on their suitability in inferring fAPAR (structural related indices) and LUE (physiologically-related indices) parameters. R denotes the reflectance at the specified wavelength (nm). NDVI: normalized difference vegetation index; MTCI: MERIS terrestrial chlorophyll index; NDI: normalized difference index; sPRI: scaled Photochemical Reflectance Index; Fy760: apparent fluorescence yield at 760 nm.

Table 3. Results from the model evaluation one leave out cross-validation analysis across LUE model configurations and vegetation indices. Based on AICcv, the best performance among formulation test for each method is highlighted text bold.

Table 4. Abbreviations.

References

Akaike, H.: Information Theory and an Extension of the Maximum Likelihood Principle. In: Selected Papers of Hirotugu Akaike, Parzen, E., Tanabe, K., and Kitagawa, G. (Eds.), Springer Series in Statistics, Springer New York, 1998.

Anderson, D. R., Burnham, K. P., and Thompson, W. L.: Null Hypothesis Testing: Problems, Prevalence, and an Alternative, The Journal of Wildlife Management, 64, 912-923, 2000.

Baret, F., Houlès, V., and Guérif, M.: Quantification of plant stress using remote sensing observations and crop models: The case of nitrogen management, Journal of Experimental Botany, 58, 869-880, 2007.

Barton, C. V. M. and North, P. R. J.: Remote sensing of canopy light use efficiency using the photochemical reflectance index: Model and sensitivity analysis, Remote Sensing of Environment, 78, 264-273, 2001.

Bates, D. M. and Watts, D. G.: Frontmatter. In: Nonlinear Regression Analysis and Its Applications, John Wiley & Sons, Inc., 2008.

Campbell, P. K. E., Middleton, E. M., Corp, L. A., and Kim, M. S.: Contribution of chlorophyll fluorescence to the apparent vegetation reflectance, Science of The Total Environment, 404, 433-439, 2008.

Cendrero-Mateo, M. P., Carmo-Silva, A. E., Porcar-Castell, A., Hamerlynck, E. P., Papuga, S. A., and Moran, M. S.: Dynamic response of plant chlorophyll fluorescence to light, water and nutrient availability, Functional Plant Biology, doi: http://dx.doi.org/10.1071/FP15002, 2015. -, 2015.

Ciompi, S., Gentili, E., Guidi, L., and Soldatini, G. F.: The effect of nitrogen deficiency on leaf gas exchange and chlorophyll fluorescence parameters in sunflower, Plant Science, 118, 177-184, 1996.

Damm, A., Elbers, J., Erler, A., Gioli, B., Hamdi, K., Hutjes, R., Kosvancova, M., Meroni, M., Miglietta, F., Moersch, A., Moreno, J., Schickling, A., Sonnenschein, R., Udelhoven, T., van der Linden, S., Hostert, P., and Rascher, U.: Remote sensing of sun-induced fluorescence to improve modeling of diurnal courses of gross primary production (GPP), Global Change Biology, 16, 171-186, 2010.

Dash, J. and Curran, P. J.: The MERIS terrestrial chlorophyll index, International Journal of Remote Sensing, 25, 5403-5413, 2004.

Dee, D. P., Uppala, S. M., Simmons, A. J., Berrisford, P., Poli, P., Kobayashi, S., Andrae, U., Balmaseda, M. A., Balsamo, G., Bauer, P., Bechtold, P., Beljaars, A. C. M., van de Berg, L., Bidlot, J., Bormann, N., Delsol, C., Dragani, R., Fuentes, M., Geer, A. J., Haimberger, L., Healy, S. B., Hersbach, H., Hólm, E. V., Isaksen, L., Kållberg, P., Köhler, M., Matricardi, M., McNally, A. P., Monge-Sanz, B. M., Morcrette, J. J., Park, B. K., Peubey, C., de Rosnay, P., Tavolato, C., Thépaut, J. N., and Vitart, F.: The ERA-Interim reanalysis: configuration and performance of the data assimilation system, Quarterly Journal of the Royal Meteorological Society, 137, 553-597, 2011.

Di Bella, C. M., Paruelo, J. M., Becerra, J. E., Bacour, C., and Baret, F.: Effect of senescent leaves on NDVI-based estimates of fAPAR: Experimental and modelling evidences, International Journal of Remote Sensing, 25, 5415-5427, 2004.

Drolet, G. G., Middleton, E. M., Huemmrich, K. F., Hall, F. G., Amiro, B. D., Barr, A. G., Black, T. A., McCaughey, J. H., and Margolis, H. A.: Regional mapping of gross light-use efficiency using MODIS spectral indices, Remote Sensing of Environment, 112, 3064-3078, 2008.

Efron, B. and Tibshirani, R. J.: An Introduction to the Bootstrap. Chapman & Hall/CRC Monographs on Statistics & Applied Probability, 1994.

766 Filella, I., Porcar-Castell, A., Munné-Bosch, S., Bäck, J., Garbulsky, M. F., and Peñuelas, J.:
767 PRI assessment of long-term changes in carotenoids/chlorophyll ratio and short-term changes
768 in de-epoxidation state of the xanthophyll cycle, International Journal of Remote Sensing, 30,
769 4443-4455, 2009.
770 Flexas, J., Escalona, J. M., Evain, S., Gulías, J., Moya, I., Osmond, C. B., and Medrano, H.:
771 Steady-state chlorophyll fluorescence (Fs) measurements as a tool to follow variations of net
772 CO2 assimilation and stomatal conductance during water-stress in C3 plants, Physiologia
773 Plantarum, 114, 231-240, 2002.
774 Frankenberg, C., O'Dell, C., Berry, J., Guanter, L., Joiner, J., Köhler, P., Pollock, R., and
775 Taylor, T. E.: Prospects for chlorophyll fluorescence remote sensing from the Orbiting
776 Carbon Observatory-2, Remote Sensing of Environment, 147, 1-12, 2014.
777 Gamon, J. A., Peñuelas, J., and Field, C. B.: A narrow-waveband spectral index that tracks
778 diurnal changes in photosynthetic efficiency, Remote Sensing of Environment, 41, 35-44,
779 1992.
780 Gamon, J. A., Serrano, L., and Surfus, J. S.: The photochemical reflectance index: an optical
781 indicator of photosynthetic radiation use efficiency across species, functional types, and
782 nutrient levels, Oecologia, 112, 492-501, 1997.
783 Garbulsky, M. F., Peñuelas, J., Gamon, J., Inoue, Y., and Filella, I.: The photochemical
784 reflectance index (PRI) and the remote sensing of leaf, canopy and ecosystem radiation use
785 efficiencies: A review and meta-analysis, Remote Sensing of Environment, 115, 281-297,
786 2011.
787 Gelybó, G., Barcza, Z., Kern, A., and Kljun, N.: Effect of spatial heterogeneity on the
788 validation of remote sensing based GPP estimations, Agricultural and Forest Meteorology,
789 174–175, 43-53, 2013.
790 Gitelson, A. A., Peng, Y., Arkebauer, T. J., and Schepers, J.: Relationships between gross
791 primary production, green LAI, and canopy chlorophyll content in maize: Implications for
792 remote sensing of primary production, Remote Sensing of Environment, 144, 65-72, 2014.
793 Grace, J., Nichol, C., Disney, M., Lewis, P., Quaife, T., and Bowyer, P.: Can we measure
794 terrestrial photosynthesis from space directly, using spectral reflectance and fluorescence?,
795 Global Change Biology, 13, 1484-1497, 2007.
796 Guanter, L., Rossini, M., Colombo, R., Meroni, M., Frankenberg, C., Lee, J.-E., and Joiner,
797 J.: Using field spectroscopy to assess the potential of statistical approaches for the retrieval of
798 sun-induced chlorophyll fluorescence from ground and space, Remote Sensing of
799 Environment, 133, 52-61, 2013.
800 Guanter, L., Zhang, Y., Jung, M., Joiner, J., Voigt, M., Berry, J. A., Frankenberg, C., Huete,
801 A. R., Zarco-Tejada, P., Lee, J.-E., Moran, M. S., Ponce-Campos, G., Beer, C., Camps-Valls,
802 G., Buchmann, N., Gianelle, D., Klumpp, K., Cescatti, A., Baker, J. M., and Griffis, T. J.:
803 Global and time-resolved monitoring of crop photosynthesis with chlorophyll fluorescence,
804 Proceedings of the National Academy of Sciences, 111, E1327-E1333, 2014.
805 Hall, F. G., Hilker, T., Coops, N. C., Lyapustin, A., Huemmrich, K. F., Middleton, E.,
806 Margolis, H., Drolet, G., and Black, T. A.: Multi-angle remote sensing of forest light use
807 efficiency by observing PRI variation with canopy shadow fraction, Remote Sensing of
808 Environment, 112, 3201-3211, 2008.
809 Heinsch, F. A., Maosheng, Z., Running, S. W., Kimball, J. S., Nemani, R. R., Davis, K. J.,
810 Bolstad, P. V., Cook, B. D., Desai, A. R., Ricciuto, D. M., Law, B. E., Oechel, W. C.,
811 Hyojung, K., Hongyan, L., Wofsy, S. C., Dunn, A. L., Munger, J. W., Baldocchi, D. D.,
812 Liukang, X., Hollinger, D. Y., Richardson, A. D., Stoy, P. C., Siqueira, M. B. S., Monson, R.
813 K., Burns, S. P., and Flanagan, L. B.: Evaluation of remote sensing based terrestrial
814 productivity from MODIS using regional tower eddy flux network observations, Geoscience
815 and Remote Sensing, IEEE Transactions on, 44, 1908-1925, 2006.

Hilker, T., Coops, N. C., Hall, F. G., Black, T. A., Wulder, M. A., Nesic, Z., and Krishnan, P.: Separating physiologically and directionally induced changes in PRI using BRDF models, Remote Sensing of Environment, 112, 2777-2788, 2008.
Hirose, T. and Werger, M. J. A.: Photosynthetic capacity and nitrogen partitioning among species in the canopy of a herbaceous plant community, Oecologia, 100, 203-212, 1994.
Huang, Z. A., Jiang, D. A., Yang, Y., Sun, J. W., and Jin, S. H.: Effects of Nitrogen Deficiency on Gas Exchange, Chlorophyll Fluorescence, and Antioxidant Enzymes in Leaves of Rice Plants, Photosynthetica, 42, 357-364, 2004.
Janssen, P. H. M. and Heuberger, P. S. C.: Calibration of process-oriented models, Ecological Modelling, 83, 55-66, 1995.
Joiner, J., Guanter, L., Lindstrot, R., Voigt, M., Vasilkov, A. P., Middleton, E. M., Huemmrich, K. F., Yoshida, Y., and Frankenberg, C.: Global monitoring of terrestrial chlorophyll fluorescence from moderate-spectral-resolution near-infrared satellite measurements: methodology, simulations, and application to GOME-2, Atmos. Meas. Tech., 6, 2803-2823, 2013.
Krause, G. H. and Weis, E.: Chlorophyll fluorescence as a tool in plant physiology, Photosynth Res, 5, 139-157, 1984.
Lee, J.-E., Frankenberg, C., van der Tol, C., Berry, J. A., Guanter, L., Boyce, C. K., Fisher, J. B., Morrow, E., Worden, J. R., Asefi, S., Badgley, G., and Saatchi, S.: Forest productivity and water stress in Amazonia: observations from GOSAT chlorophyll fluorescence, 2013.
Madani, N., Kimball, J. S., Affleck, D. L. R., Kattge, J., Graham, J., van Bodegom, P. M., Reich, P. B., and Running, S. W.: Improving ecosystem productivity modeling through spatially explicit estimation of optimal light use efficiency, Journal of Geophysical Research: Biogeosciences, 119, 2014JG002709, 2014.
Mänd, P., Hallik, L., Peñuelas, J., Nilson, T., Duce, P., Emmett, B. A., Beier, C., Estiarte, M., Garadnai, J., Kalapos, T., Schmidt, I. K., Kovács-Láng, E., Prieto, P., Tietema, A., Westerveld, J. W., and Kull, O.: Responses of the reflectance indices PRI and NDVI to experimental warming and drought in European shrublands along a north–south climatic gradient, Remote Sensing of Environment, 114, 626-636, 2010.
McMurtrey, J. E., Middleton, E. M., Corp, L. A., Campbell, P., Butcher, L. M., and Daughtry, C. S. T.: Optical reflectance and fluorescence for detecting nitrogen needs in Zea mays L, 21-25 July 2003 2003, 4602-4604 vol.4607.
Meroni, M., Barducci, A., Cogliati, S., Castagnoli, F., Rossini, M., Busetto, L., Migliavacca, M., Cremonese, E., Galvagno, M., Colombo, R., and di Cella, U. M.: The hyperspectral irradiometer, a new instrument for long-term and unattended field spectroscopy measurements, Review of Scientific Instruments, 82, -, 2011.
Meroni, M., Busetto, L., Colombo, R., Guanter, L., Moreno, J., and Verhoef, W.: Performance of Spectral Fitting Methods for vegetation fluorescence quantification, Remote Sensing of Environment, 114, 363-374, 2010.
Meroni, M. and Colombo, R.: 3S: A novel program for field spectroscopy, Computers & Geosciences, 35, 1491-1496, 2009.
Migliavacca, M., Galvagno, M., Cremonese, E., Rossini, M., Meroni, M., Sonnentag, O., Cogliati, S., Manca, G., Diotri, F., Busetto, L., Cescatti, A., Colombo, R., Fava, F., Morra di Cella, U., Pari, E., Siniscalco, C., and Richardson, A. D.: Using digital repeat photography and eddy covariance data to model grassland phenology and photosynthetic CO2 uptake, Agricultural and Forest Meteorology, 151, 1325-1337, 2011.
Monteith, J. L.: Solar Radiation and Productivity in Tropical Ecosystems, Journal of Applied Ecology, 9, 747-766, 1972.
Musavi, T., Mahecha, M. D., Migliavacca, M., Reichstein, M., van de Weg, M. J., van Bodegom, P. M., Bahn, M., Wirth, C., Reich, P. B., Schrodt, F., and Kattge, J.: The imprint of

plants on ecosystem functioning: A data-driven approach, International Journal of Applied Earth Observation and Geoinformation, 43, 119-131, 2015.
Nichol, C. J., Huemmrich, K. F., Black, T. A., Jarvis, P. G., Walthall, C. L., Grace, J., and Hall, F. G.: Remote sensing of photosynthetic-light-use efficiency of boreal forest, Agricultural and Forest Meteorology, 101, 131-142, 2000.
Parazoo, N. C., Bowman, K., Fisher, J. B., Frankenberg, C., Jones, D. B. A., Cescatti, A., Pérez-Priego, Ó., Wohlfahrt, G., and Montagnani, L.: Terrestrial gross primary production inferred from satellite fluorescence and vegetation models, Global Change Biology, 20, 3103-3121, 2014.
Peñuelas, J., Garbulsky, M. F., and Filella, I.: Photochemical reflectance index (PRI) and remote sensing of plant CO2 uptake, New Phytologist, 191, 596-599, 2011.
Peñuelas, J., Poulter, B., Sardans, J., Ciais, P., van der Velde, M., Bopp, L., Boucher, O., Godderis, Y., Hinsinger, P., Llusia, J., Nardin, E., Vicca, S., Obersteiner, M., and Janssens, I. A.: Human-induced nitrogen–phosphorus imbalances alter natural and managed ecosystems across the globe, Nat Commun, 4, 2013.
Pérez-Priego, O., López-Ballesteros, A., Sánchez-Cañete, E., Serrano-Ortiz, P., Kutzbach, L., Domingo, F., Eugster, W., and Kowalski, A.: Analysing uncertainties in the calculation of fluxes using whole-plant chambers: random and systematic errors, Plant and Soil, doi: 10.1007/s11104-015-2481-x, 2015. 1-16, 2015.
Pérez-Priego, O., Zarco-Tejada, P. J., Miller, J. R., Sepulcre-Cantó, G., and Fereres, E.: Detection of water stress in orchard trees with a high-resolution spectrometer through chlorophyll fluorescence In-Filling of the O 2-A band, IEEE Transactions on Geoscience and Remote Sensing, 43, 2860-2868, 2005.
Porcar-Castell, A., Garcia-Plazaola, J., Nichol, C., Kolari, P., Olascoaga, B., Kuusinen, N., Fernández-Marín, B., Pulkkinen, M., Juurola, E., and Nikinmaa, E.: Physiology of the seasonal relationship between the photochemical reflectance index and photosynthetic light use efficiency, Oecologia, 170, 313-323, 2012.
Porcar-Castell, A., Mac Arthur, A., Rossini, M., Eklundh, L., Pacheco-Labrador, J., Anderson, K., Balzarolo, M., Martín, M. P., Jin, H., Tomelleri, E., Cerasoli, S., Sakowska, K., Hueni, A., Julitta, T., Nichol, C. J., and Vescovo, L.: EUROSPEC: at the interface between remote sensing and ecosystem CO2 flux measurements in Europe, Biogeosciences Discuss., 12, 13069-13121, 2015.
Prince, S. D. and Goward, S. N.: Global Primary Production: A Remote Sensing Approach, Journal of Biogeography, 22, 815-835, 1995.
Raessler, M., Rothe, J., and Hilke, I.: Accurate determination of Cd, Cr, Cu and Ni in woodlice and their skins—is moulting a means of detoxification?, Science of The Total Environment, 337, 83-90, 2005.
Rahman, A. F., Cordova, V. D., Gamon, J. A., Schmid, H. P., and Sims, D. A.: Potential of MODIS ocean bands for estimating CO2 flux from terrestrial vegetation: A novel approach, Geophysical Research Letters, 31, L10503, 2004.
Reichstein, M., Bahn, M., Mahecha, M. D., Kattge, J., and Baldocchi, D. D.: Linking plant and ecosystem functional biogeography, Proceedings of the National Academy of Sciences, 111, 13697-13702, 2014.
Rossini, M., Cogliati, S., Meroni, M., Migliavacca, M., Galvagno, M., Busetto, L., Cremonese, E., Julitta, T., Siniscalco, C., di Cella, U. M., and Colombo, R.: Remote sensing-based estimation of gross primary production in a subalpine grassland, Biogeosciences, 9, 2565-2584, 2012.
Rossini, M., Meroni, M., Migliavacca, M., Manca, G., Cogliati, S., Busetto, L., Picchi, V., Cescatti, A., Seufert, G., and Colombo, R.: High resolution field spectroscopy measurements

for estimating gross ecosystem production in a rice field, Agricultural and Forest Meteorology, 150, 1283-1296, 2010.
Rossini, M., Migliavacca, M., Galvagno, M., Meroni, M., Cogliati, S., Cremonese, E., Fava, F., Gitelson, A., Julitta, T., Morra di Cella, U., Siniscalco, C., and Colombo, R.: Remote estimation of grassland gross primary production during extreme meteorological seasons, International Journal of Applied Earth Observation and Geoinformation, 29, 1-10, 2014.
Rossini, M., Nedbal, L., Guanter, L., Ač, A., Alonso, L., Burkart, A., Cogliati, S., Colombo, R., Damm, A., Drusch, M., Hanus, J., Janoutova, R., Julitta, T., Kokkalis, P., Moreno, J., Novotny, J., Panigada, C., Pinto, F., Schickling, A., Schüttemeyer, D., Zemek, F., and Rascher, U.: Red and far red Sun-induced chlorophyll fluorescence as a measure of plant photosynthesis, Geophysical Research Letters, 42, 1632-1639, 2015.
Rouse, J. W., Haas, R. H., Schell, J. A., Deering, D. W., and Harlan, J. C.: Monitoring the vernal advancements and retro gradation of natural vegetation, Greenbelt, MD, USA., 1974. 1974.
Ruimy, A., Saugier, B., and Dedieu, G.: Methodology for the estimation of terrestrial net primary production from remotely sensed data, Journal of Geophysical Research, 99, 5263 - 5283, 1994.
Schlemmer, M., Gitelson, A., Schepers, J., Ferguson, R., Peng, Y., Shanahan, J., and Rundquist, D.: Remote estimation of nitrogen and chlorophyll contents in maize at leaf and canopy levels, International Journal of Applied Earth Observation and Geoinformation, 25, 47-54, 2013.
Suárez, L., Zarco-Tejada, P. J., Sepulcre-Cantó, G., Pérez-Priego, O., Miller, J. R., Jiménez-Muñoz, J. C., and Sobrino, J.: Assessing canopy PRI for water stress detection with diurnal airborne imagery, Remote Sensing of Environment, 112, 560-575, 2008.
Sugiharto, B., Miyata, K., Nakamoto, H., Sasakawa, H., and Sugiyama, T.: Regulation of Expression of Carbon-Assimilating Enzymes by Nitrogen in Maize Leaf, Plant Physiology, 92, 963-969, 1990.
Tremblay, N., Wang, Z., and Cerovic, Z.: Sensing crop nitrogen status with fluorescence indicators. A review, Agron. Sustain. Dev., 32, 451-464, 2012.
Walker, A. P., Beckerman, A. P., Gu, L., Kattge, J., Cernusak, L. A., Domingues, T. F., Scales, J. C., Wohlfahrt, G., Wullschleger, S. D., and Woodward, F. I.: The relationship of leaf photosynthetic traits – Vcmax and Jmax – to leaf nitrogen, leaf phosphorus, and specific leaf area: a meta-analysis and modeling study, Ecology and Evolution, 4, 3218-3235, 2014.
Wang, W., Yao, X., Yao, X., Tian, Y., Liu, X., Ni, J., Cao, W., and Zhu, Y.: Estimating leaf nitrogen concentration with three-band vegetation indices in rice and wheat, Field Crops Research, 129, 90-98, 2012.
Yuan, W., Cai, W., Liu, S., Dong, W., Chen, J., Arain, M. A., Blanken, P. D., Cescatti, A., Wohlfahrt, G., Georgiadis, T., Genesio, L., Gianelle, D., Grelle, A., Kiely, G., Knohl, A., Liu, D., Marek, M. V., Merbold, L., Montagnani, L., Panferov, O., Peltoniemi, M., Rambal, S., Raschi, A., Varlagin, A., and Xia, J.: Vegetation-specific model parameters are not required for estimating gross primary production, Ecological Modelling, 292, 1-10, 2014.
Zarco-Tejada, P. J., Suarez, L., and Gonzalez-Dugo, V.: Spatial Resolution Effects on Chlorophyll Fluorescence Retrieval in a Heterogeneous Canopy Using Hyperspectral Imagery and Radiative Transfer Simulation, Geoscience and Remote Sensing Letters, IEEE, 10, 937-941, 2013.

Campaign	Treatment	Total PAIg (m^2 m^{-2})	Total PAIg (m^2 m^{-2})	Forbs f_{PAI}	Grass f_{PAI}	legumes f_{PAI}	Total C content (mg g^{-1})	Total C content (mg g^{-1})	Total N content (mg g^{-1})	Total N content (mg g^{-1})	Total P content (mg g^{-1})	Total P content (mg g^{-1})	N/P (mg g^{-1})
Date	--	mean	SD	%	%	%	mean	SD	mean	SD	mean	SD	--
#1 March 20 th, 2014 Growing period Pre-treatment	C	0.85	0.18	35.5	56.8	7.7	425	--	17.7	--	2.08	--	8.5
	N	0.76	0.21	39.2	45.1	15.0	463	--	18.6	--	1.99	--	9.34
	NP	1.03	0.30	29.1	54.3	12.9	421	--	18.1	--	1.90	--	9.52
	P	0.95	0.21	26.6	66.6	6.9	369	--	16.9	--	1.94	--	8.71
#2 April 15 th, 2014 Growing period Post-treatment	C	2.02	0.43	14.5	85.2	0.3	413	152	14.6	0.8	2.23	0.02	6.6
	N	2.17	0.91	11.9	87.6	0.4	384	121	23.7	2.0	1.68	0.03	14.2
	NP	2.46	0.45	4.1	95.6	0.3	377	330	23.5	4.1	3.95	0.04	6.0
	P	1.66	0.58	14.2	85.7	0.1	394	212	15.4	1.7	4.22	0.06	3.7
#3 May 7 th, 2014 Dry period	C	1.08	0.27	43.0	55.1	1.9	447	52	14.2	1.3	2.41	0.02	5.9
	N	1.29	0.58	28.3	70.7	1.0	449	114	20.1	3.1	1.86	0.03	10.8
	NP	0.84	0.21	27.2	71.8	1.0	438	64	20.6	1.2	3.50	0.04	5.9
	P	1.37	0.57	39.5	58.5	2.0	444	206	14.7	0.8	3.83	0.03	3.8
#4 May 27 th, 2014 Dry period	C	0.44	0.10	66.7	33.3	0.0	442	2	13.8	1.2	2.12	0.01	6.5
	N	0.48	0.28	36.4	63.6	0.0	448	3	19.0	2.8	1.93	0.02	9.8
	NP	0.53	0.26	40.6	59.4	0.0	442	1	18.5	3.4	2.63	0.02	7.1
	P	0.71	0.31	56.1	43.9	0.0	441	72	13.2	0.7	2.62	0.02	5.0

Table 1. Ancillary data resulting from the analysis. Green Plant Area Index (PAIg), fraction of PAI in different plant forms (fPAI), and C, N, and P plant content. The N:P ratio also is shown. Data correspond to the mean value and standard deviation (SD) of the subsamples taken in each plot and treatment.

Index	Target	Model proxy	Formulation	References
NDVI	*Green biomass & Leaf area*	f_{APAR}	$(R_{800}-R_{680})/(R_{800}+R_{680})$	Rouse et al., 1974
MTCI	*Chlorophyll & Nitrogen content*	f_{APAR}	$(R_{754} - R_{709})/(R_{709} - R_{681})$	Dash and Curran, 2004
sPRI	Physiology	LUE	$(R_{531}-R_{570})/(R_{531}+R_{570})$	Gamon et al., 1992
Fy_{760}	Physiology	LUE	Chlorophyll Fluorescence In-Filling of the O_2-A Band	Meroni and Colombo, 2006

Table 2. Spectral vegetation indices computed in this study. Vegetation indices are classified into two major classes based on their suitability in inferring fAPAR (structural related indices) and LUE (physiologically-related indices) parameters. R denotes the reflectance at the specified wavelength (nm). NDVI: normalized difference vegetation index; MTCI: MERIS terrestrial chlorophyll index; NDI: normalized difference index; sPRI: scaled Photochemical Reflectance Index; Fy760: apparent fluorescence yield at 760 nm.

LUE Model	Variable	RMSE	rRMSE	r2	ME	RMSEcv	rRMSEcv	r2cv	MEcv	AICcv
MM-VPD	NDVI	3.041	23.439	0.894	0.802	3.143	24.671	0.877	0.788	160.887
MM-SWC	NDVI	2.663	32.909	0.849	0.848	2.769	34.840	0.835	0.829	148.417
MM (VPD-SWC)	**NDVI**	**2.230**	**21.727**	**0.894**	**0.893**	**2.357**	**23.266**	**0.881**	**0.879**	**127.478**
RSM	**PRI-NDVI**	**2.390**	**24.112**	**0.879**	**0.877**	**2.760**	**30.832**	**0.844**	**0.837**	**140.627**
RSM	PRI-MTCI	3.113	35.793	0.794	0.792	3.489	42.123	0.751	0.739	171.125
RSM	**Fy760-NDVI**	**2.490**	**27.743**	**0.868**	**0.867**	**2.835**	**34.242**	**0.834**	**0.828**	**144.116**
RSM	Fy760-MTCI	3.676	46.770	0.710	0.710	4.074	52.224	0.654	0.644	191.275

Table 3. Results from the model evaluation one leave out cross validation analysis across LUE model configurations and vegetation indices. Based on AICcv, the best performance among formulation test for each method is highlighted text bold.

Table 4. List of abbreviations

a, **a_o**, and **a_1** are model parameters; **b_0**, **b_1**, **b_2**, and **b_3** are fitting parameters of RSM; **EFPs**, ecosystem functional properties; ***f*(meteo),** limiting functions relying on meteorologically-driven data; ***f*APAR**, fraction of absorbed photosynthetically active radiation; ***f*PAIg**, fraction of *PAIg* in different plant forms; **Fy760**, sun-induced chlorophyll Fluorescence yield at 760 nm; **GPP**, gross primary productivity; **GPP_{noon}**: instantaneous gross photosynthetic rate taken at solar noon (between 11:00 and 15:00 pm solar time); GPP_{daily}: mean value of the diurnal time course of gross photosynthetic rate; **GPP_{2000}**, gross primary productivity estimated at 2000 of PAR; **LUE,** light use-efficiency; **LUE_m** potential or maximum LUE; **MM**, meteorologically driven model; **MM-VPD,** simplifier model of the original MOD17 that account for VPD in *f*(meteo); **MM(SWC-VPD)** meteorologically-driven model that account for VPD and soil moisture in *f*(meteo); **MTCI**, MERIS terrestrial-chlorophyll index; **NDVI**, Normalized difference vegetation index; **NEE**, net ecosystem CO_2 exchange; **PAIg**, Green Plant Area Index; **PAR**, Photosynthetically active radiation; ***ph***, physiologically-related parameter of RSM referring to either sPRI or Fy760 as a proxy for LUE; **PLRC**, photosynthetic light response curve; **PRI**, photochemical reflectance index; **R_{eco}**, daytime ecosystem respiration; **RSM**, remote sensing based models; **SIF**, sun-induced chlorophyll fluorescence; **sPRI**, scaled-photochemical reflectance index; ***st***, structurally-related parameter of RSM referring to either NDVI or MTCI as a proxy for *f*APAR; **SWC**, soil water content; **SWC_{max}** parameter of the *f(meteo)* term; **VPD**, air-to-leaf vapor pressure deficit; **VPD_{max}** and **VPD_{min}** are fitting parameters of the *f(meteo)* term; $\boldsymbol{\alpha}$ is a parameter describing the photosynthetic quantum yield; $\boldsymbol{\beta}$ is the parameter that extrapolates to GPP at saturating light condition.

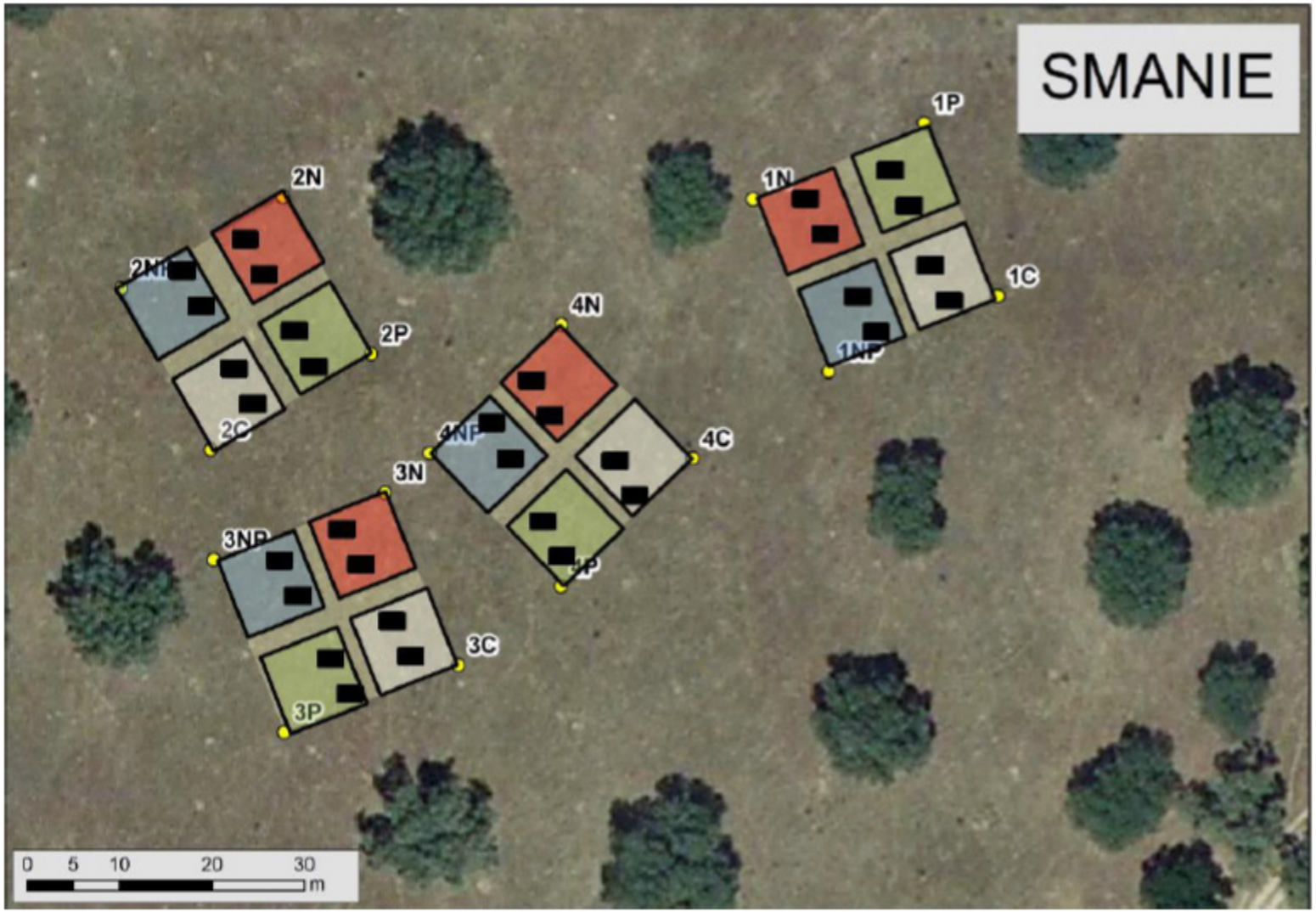

Fig. 1

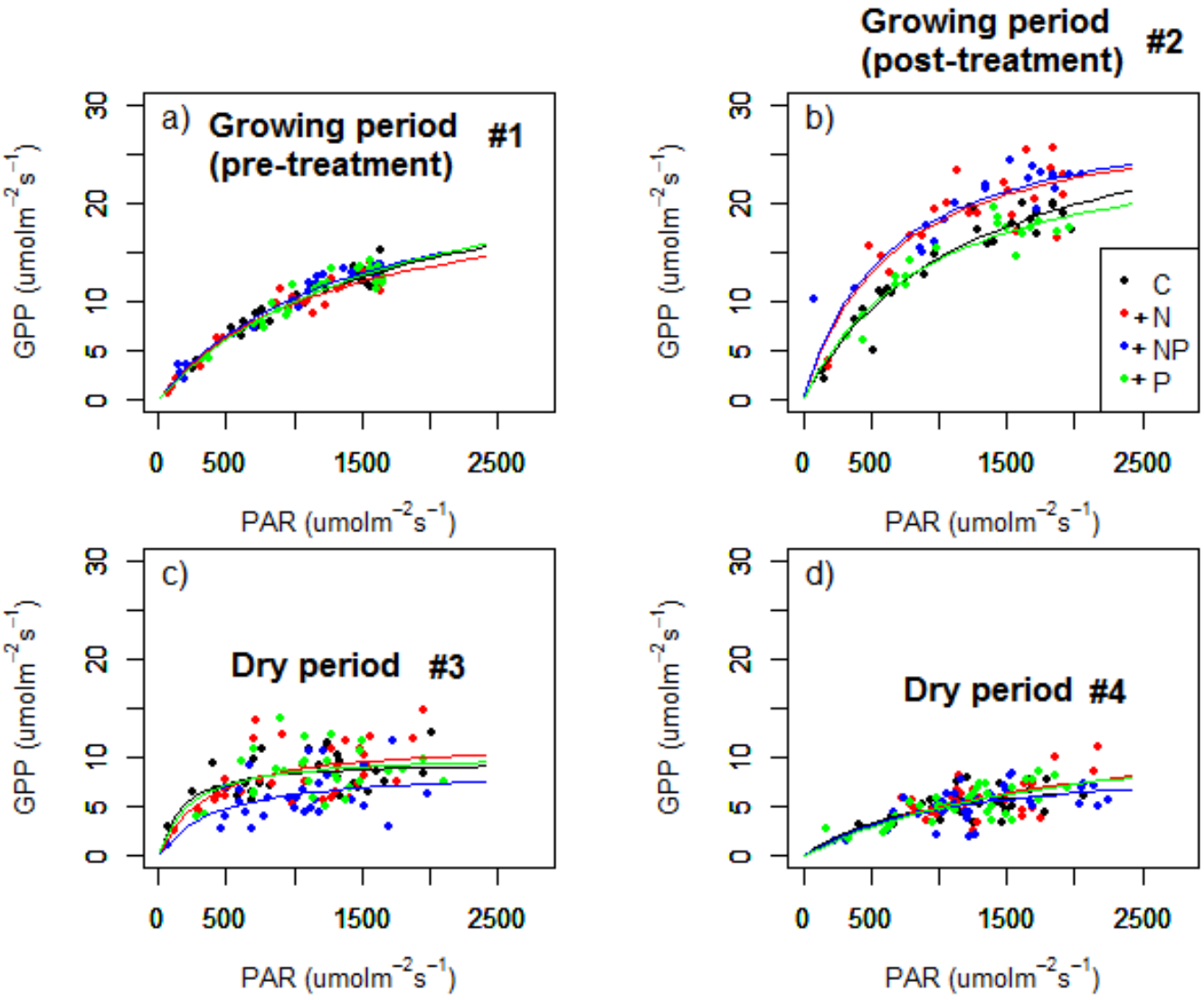
a)
Growing period
(pre-treatment)
#1
b)
Growing period
(post-treatment)
#2
c)
Dry period
#3
d)
Dry period
#4
C
+ N
+ NP
+ P
GPP (umolm^{-2}s^{-1})
PAR (umolm^{-2}s^{-1})
0
5
10
20
30
500
1500
2500

Fig. 2

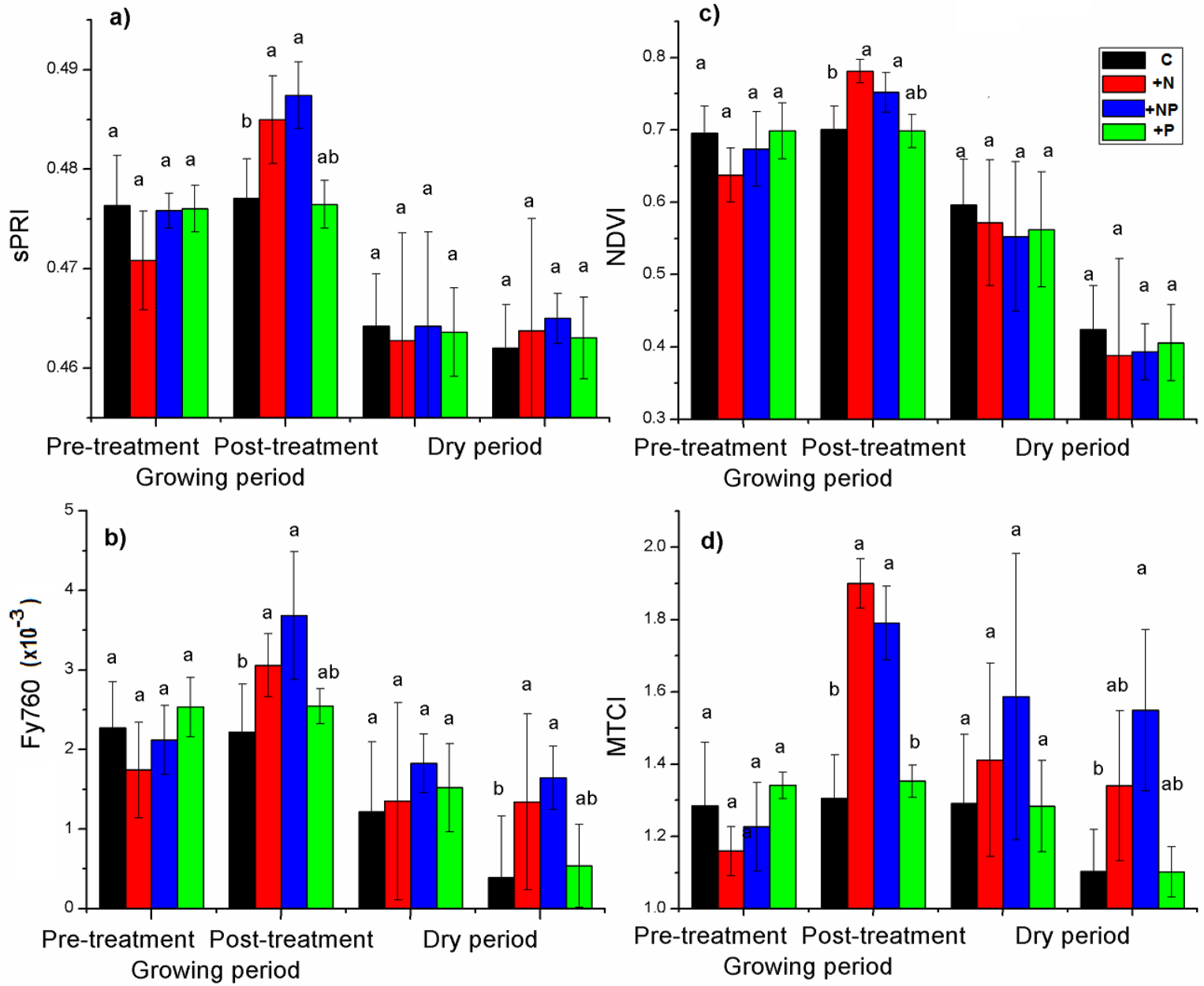
a)
sPRI
0.49
0.48
0.47
0.46
Pre-treatment
Post-treatment
Dry period
Growing period
c)
NDVI
0.8
0.7
0.6
0.5
0.4
0.3
C
+N
+NP
+P
b)
Fy760 (x10-3)
5
4
3
2
1
0
d)
MTCI
2.0
1.8
1.6
1.4
1.2
1.0

Fig. 3

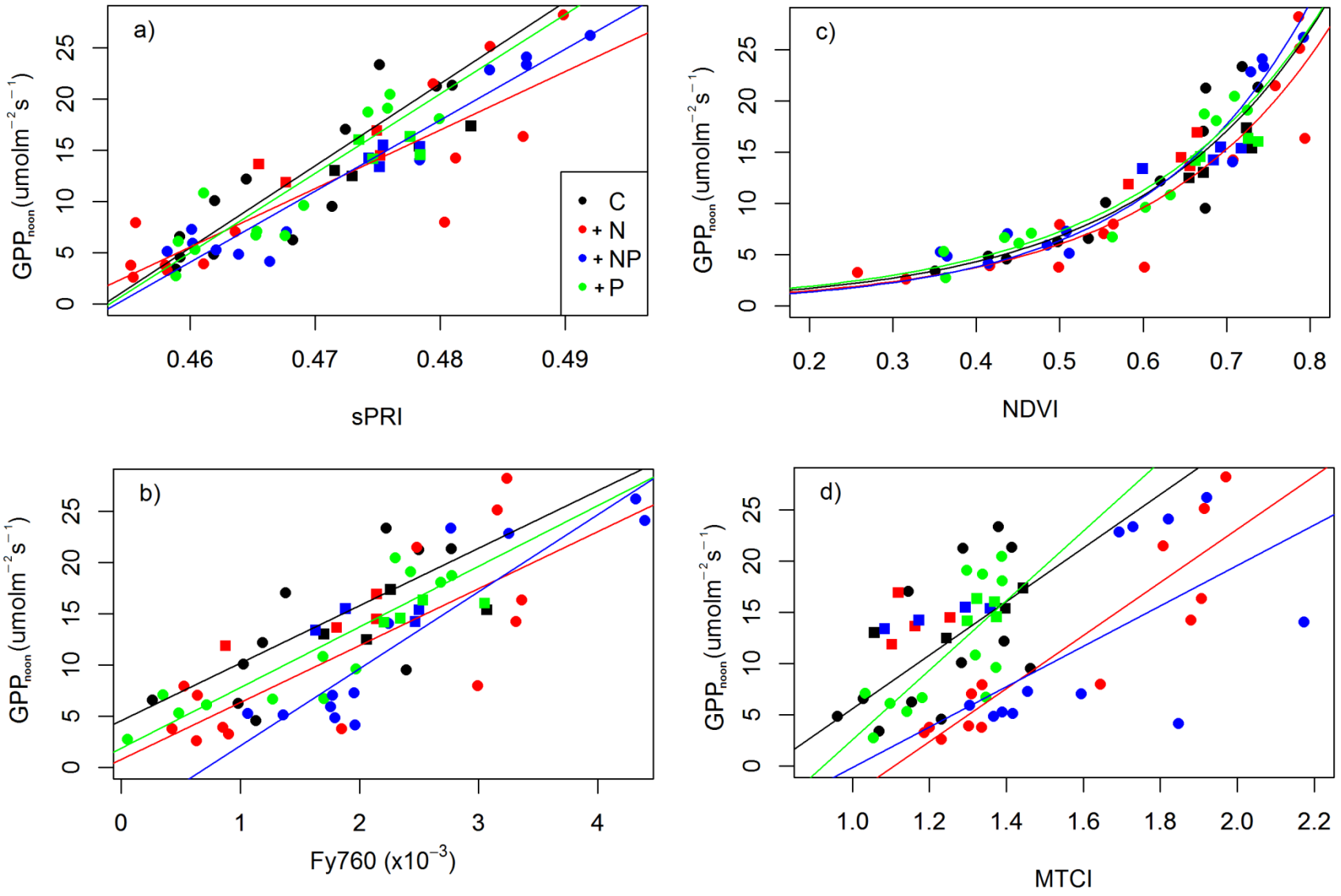

Fig. 4

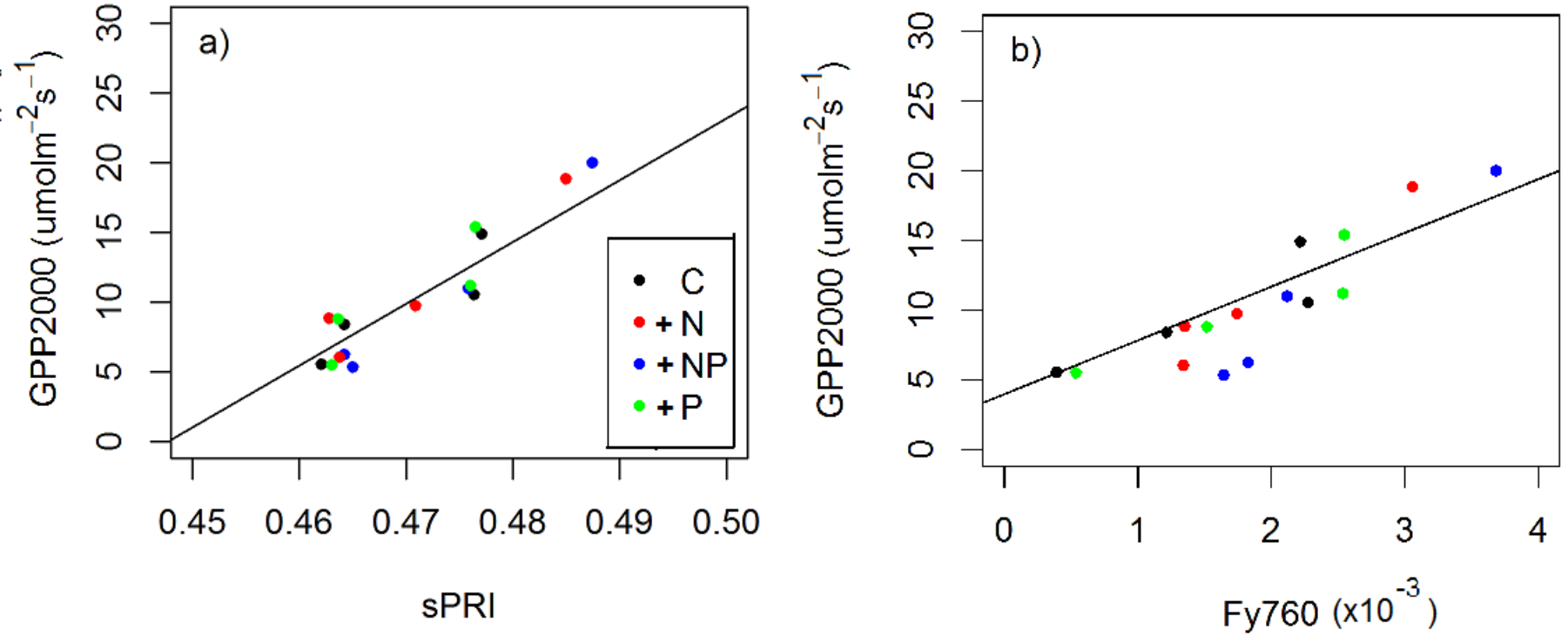
a)
GPP2000 (umolm^{-2}s^{-1})
0
5
10
15
20
25
30
0.45
0.46
0.47
0.48
0.49
0.50
sPRI
C
+ N
+ NP
+ P
b)
GPP2000 (umolm^{-2}s^{-1})
0
1
2
3
4
Fy760 (x10^{-3})

Fig. 5

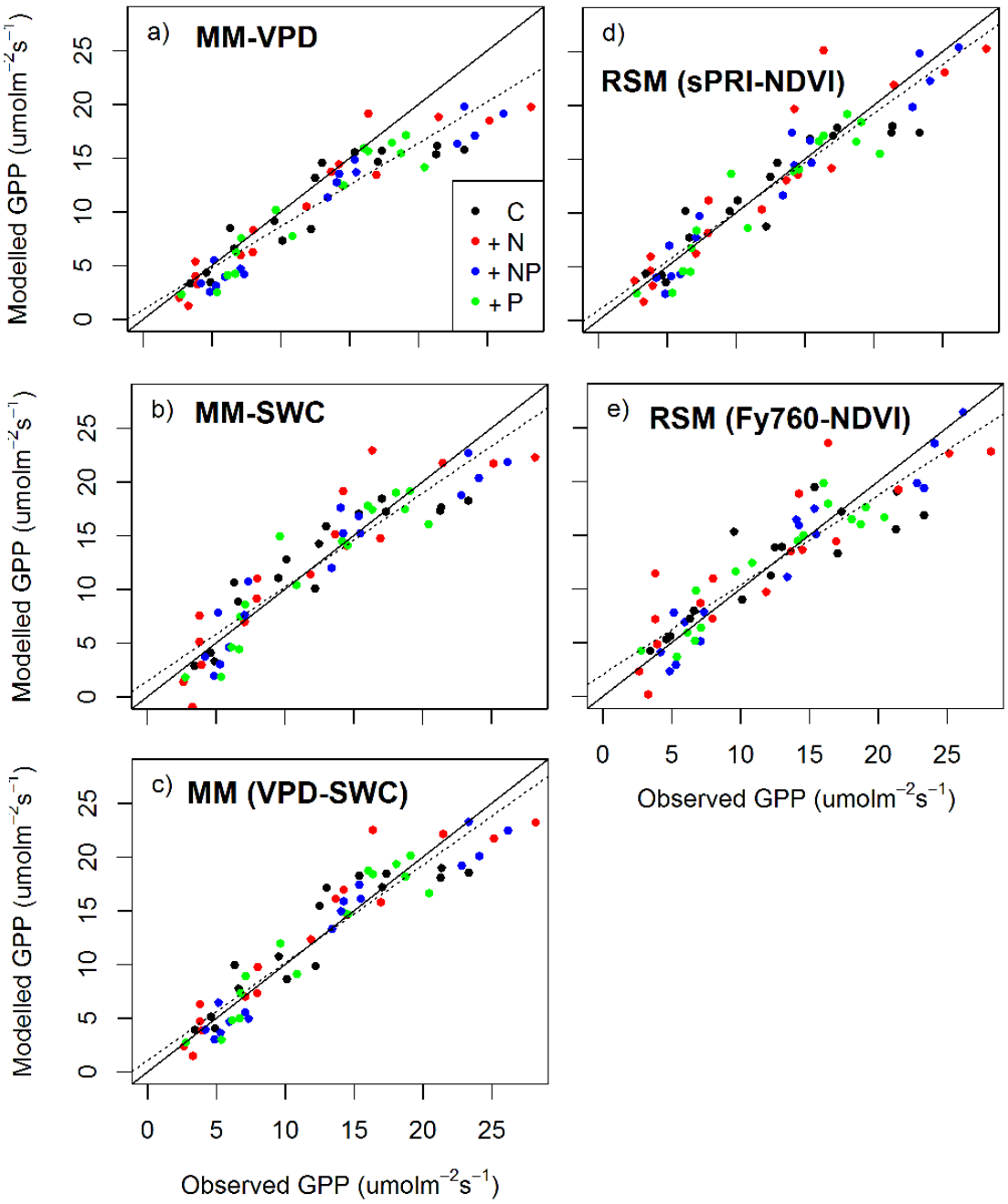
a) MM-VPD
b) MM-SWC
c) MM (VPD-SWC)
d) RSM (sPRI-NDVI)
e) RSM (Fy760-NDVI)
C
+ N
+ NP
+ P
Modelled GPP (umolm^{-2}s^{-1})
Observed GPP (umolm^{-2}s^{-1})
0
5
10
15
20
25

Fig. 6

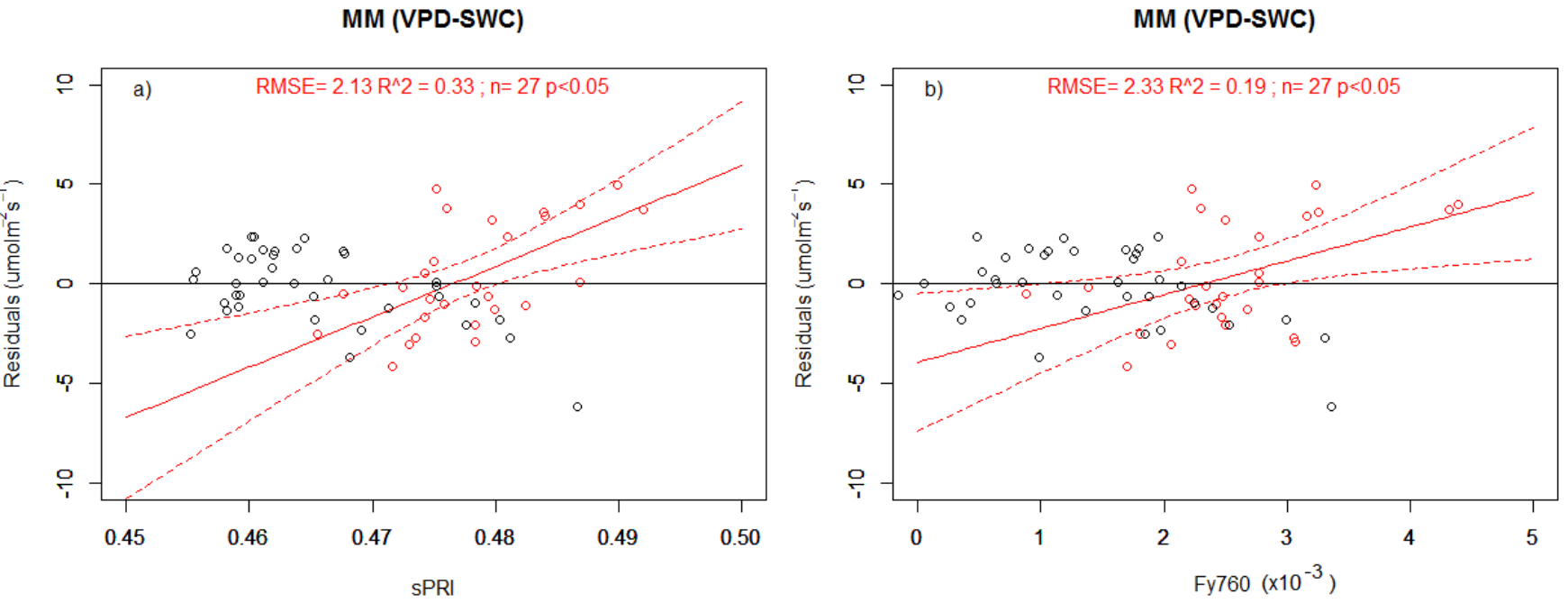
MM (VPD-SWC)
a)
RMSE= 2.13 R^2 = 0.33 ; n= 27 p<0.05
Residuals (umolm-2s-1)
10
5
0
-5
-10
0.45
0.46
0.47
0.48
0.49
0.50
sPRI
MM (VPD-SWC)
b)
RMSE= 2.33 R^2 = 0.19 ; n= 27 p<0.05
Residuals (umolm-2s-1)
0
1
2
3
4
5
Fy760 (x10-3)

Fig. 7

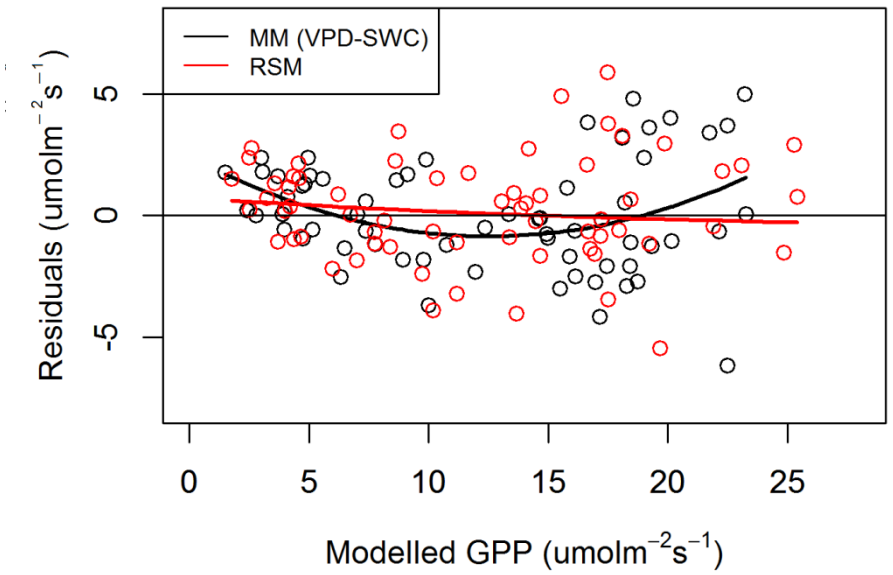
MM (VPD-SWC)
RSM
Residuals (umolm^{-2}s^{-1})
5
0
-5
0
5
10
15
20
25
Modelled GPP (umolm^{-2}s^{-1})

Fig. 8

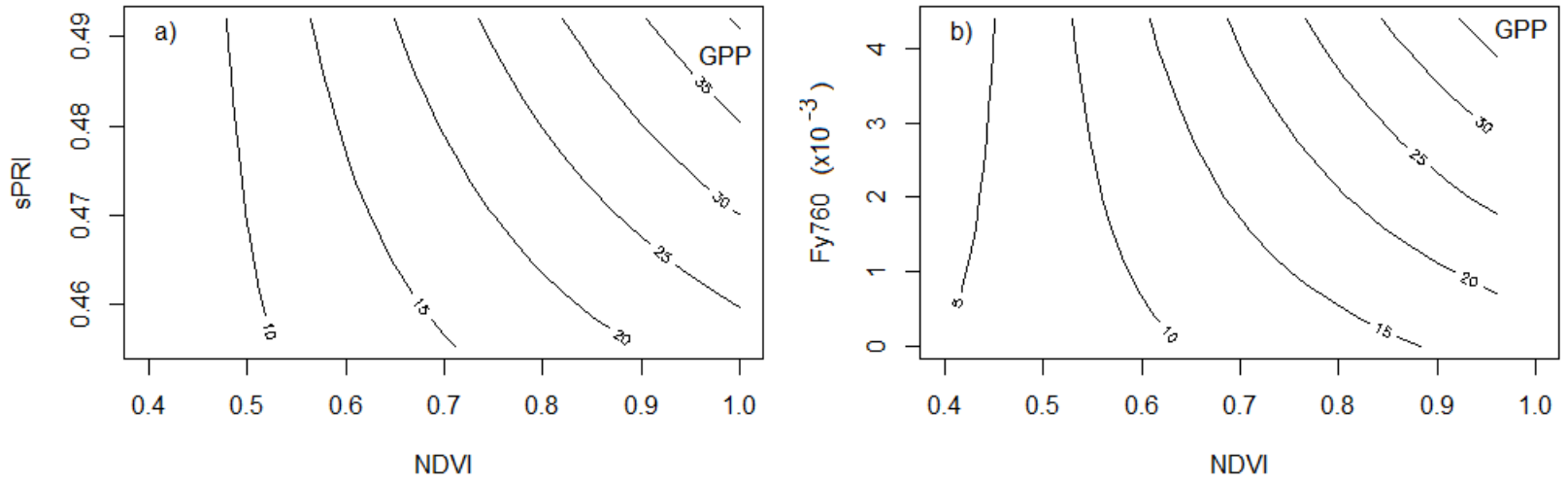
a)
GPP
sPRI
0.46
0.47
0.48
0.49
0.4
0.5
0.6
0.7
0.8
0.9
1.0
NDVI
10
15
20
25
30
35
b)
GPP
Fy760 (x10 -3)
0
1
2
3
4
NDVI
5
10
15
20
25
30

Fig. 9